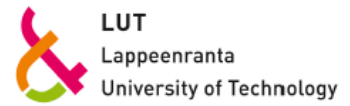LAPPEENRANTA UNIVERSITY OF TECHNOLOGY

LUT School of Engineering Science

Degree Program of Chemical Engineering

Master's Thesis

2017

Robert Heikkinen

MULTIPHASE FLOW IN INDUSTRIAL SCALE DRAFT TUBE REACTOR

Examiners: Professor, DSc (Tech) Tuomas Koiranen
               DSc (Tech) Johanna Vaittinen
               MSc (Tech) Marko Latva-Kokko

Instructors: MSc (Tech) Dmitry Gradov
               MSc (Tech) Mei Han

FOREWORDS

This Master's thesis was done in Lappeenranta University of Technology between June and November 2017.

This project was a leap to unknown for someone who has never touched CFD before and I would like to thank Tuomas Koiranen for providing me with the chance to learn something new. I would also like to express my deepest gratitude to Dmitry Gradov for having the patience to teach and guide me and answer my infinite questions that came along the learning process regarding CFD. Special thanks goes to Mei Han for providing the geometry and new mesh based on my requests and helping out with UDFs. Many thanks also to the industrial associates from Outotec, Marko Latva-Kokko and Neste Jacobs, Johanna Vaittinen for providing me with such good criticism and insights and also expressing the needs from industrial point of view.

I would also like to thank my friends and family for supporting me and giving me the chance to take a break from working every now and then. Also a special thanks to Chelsea Football Club for giving me something to look forward to almost on a weekly basis.

Lappeenranta, 16th of November, 2017.
Robert Heikkinen

ABSTRACT

Lappeenranta University of Technology
School of Engineering Science
Degree Program of Chemical Engineering

Robert Heikkinen
Multiphase Flow in Industrial Scale Draft Tube Reactor

Master's thesis
2017

83 pages, 36 figures, 16 tables

Examiners: Professor, DSc (Tech) Tuomas Koiranen
DSc (Tech) Johanna Vaittinen
MSc (Tech) Marko Latva-Kokko

Keywords: CFD, dispersion, Fluent, gas-liquid, scale-up

In this thesis, industrial scale draft tube reactor was simulated with a commercial computation fluid dynamics (CFD)-software, ANSYS Fluent 18.0. Gas-liquid mixing was simulated in a commercial reactor, OKTOP®9000, agitated draft tube reactor ($985m^3$). The geometry of the reactor was created in laboratory scale earlier for FERMATRA studies, which was then scaled-up with some modifications to improve simulation stability. Euler-Euler steady-state per-phase model was used to simulate the gas-liquid process. Phases that were considered in the simulation were water-ethanol 3% solution (continuous phase) and air (dispersed phase). Impeller was modeled with impeller boundary condition model (IBC). The literature part of this thesis reviews CFD simulations regarding scale-up and general scaling-up procedures for different multiphase processes with the emphasis on agitated vessel, gas-liquid and bioreactor scaling-up that are studied in this work.

The objectives of this thesis were to **(1)** study drag laws that could be applied to the simulation process, **(2)** make sensitivity analysis on the effect of bubble size, **(3)** perform an analysis on the flooding point, **(4)** analyze how gas feed affects the mass transfer and **(5)** develop a method for a utility scale model that can be achieved in realistic computational time.

The most important interfacial interphase force in this kind of system is the force which acts on the bubbles that is a result from the mean relative velocity between phases, the turbulent drag force. Gas-liquid stirred vessels are dominated by drag, buoyancy and convection. Since the reactor in this study had a relatively low gas volume per vessel volume per minute (*vvm*) only drag force had the most significant impact on the flow and other forces such as lift force and added mass force were negligible. The drag model that was used for the simulations was Schiller-Naumann with Lane's correlation that counts for relative velocity between phases. Also, the effect of swarm of bubbles by Roghair *et al.* (2013) was implemented to the Lane's correlation.

The steady-state simulations took ~18h (3.70GHz quad-core processor and 8GB RAM) each and were done with average bubble size of 3mm and gas feeds from 1980 to 15000m^3/h. The bubble sensitivity analysis revealed that the main variables (gas hold-up and mass transfer) follow 2nd degree polynomial curve if average bubble size is changed. The flooding point was close to 9000m^3/h and mass transfer rate ranged from 0.0394 to 0.1074s^{-1} until the flooding point.

TIIVISTELMÄ

Tässä työssä simuloitiin monifaasi-virtaus teollisen mittakaavan imuputkireaktorissa käyttäen ANSYS Fluent 18.0 laskennallisen virtausmekaniikan (CFD) ohjelmaa. Simulaatiot perustuivat kaupalliseen imuputkireaktoriin, OKTOP®9000:een ($985m^3$). Simuloitava geometria oli aiemmassa työssä laadittu laboratorimittakoossa, joka skaalattiin isommaksi. Monifaasi-simulointeihin käytettiin Euler-Euler faasikohtaista mallia. Käytetyt faasit olivat neste (vesi-etanoli 3% liuos) ja kaasufaasi (ilma). Sekoitin oli mallinnettu reunaehtomallin (IBC) mukaisesti. Työn kirjallisuusosuudessa käydään läpi yleisiä prosessien skaalausmetodeja ja kuinka skaalaus tulee ottaa huomioon tehdessä CFD simulaatioita. Sekoitussäiliöt, kaasu-neste sekä bioreaktorit on otettu erityisesti esille tähän työhön liittyen.

Tämän työn tarkoituksena oli **(1)** tutkia väliaineen vastuslakeja, joita voitaisiin käyttää kyseisen prosessin simulointiin, **(2)** tehdä herkkyysanalyysi kuplakoon vaikutukselle, **(3)** simuloida mahdollinen sekoittimen tulviminen, **(4)** analysoida kuinka kaasunsyötön lisäys vaikuttaa faasien väliseen aineensiirtoon ja **(5)** valita sopivat menetelmät, joilla täyden mittakaavan simulaatiot voidaan toteuttaa realistisessa ajassa.

Kaasu-nestesysteemeissä tärkein faasien rajapinnalla vaikuttava voima on sellainen, joka vaikuttaa kupliin. Tämä johtuu faasien välisestä suhteellisesta nopeudesta, turbulenttisesta väliaineen vastusvoimasta. Väliaineen vastus, noste ja konvektio ovat dominoivia voimia kaasu-nestesekoitussäiliöissä. Tässä työssä tutkitussa reaktorissa oli kuitenkin suhteellisen alhainen kaasun tilavuusvirta minuutissa suhteessa nesteen tilavuuteen (*vvm*), joten väliaineen vastus on ainut huomioitava voima, joka vaikuttaa nestevirtaukseen. Noste ja massan aiheuttama vastus ovat lähes olemattomia. Tämän takia simulaatioissa käytettiin väliaineen vastuksena Schiller-Naumannin mallia, jota oli muokattu Lanen korrelaatiolla. Korrelaatioon oli lisätty myös Roghairin esittämä kuplaparven vaikutus.

Yksi simulaatio kesti n.18h 3.70GHz neljän ytimen prosessoria ja 8GB RAM-muistia käyttäen. Simulaatioissa käytettiin keskiarvoista 3mm kuplakokoa ja kaasusyöttö vaihteli 1980 ja 15000m^3/h välillä. Kuplakoon herkkyysanalyysistä saatiin selville, että käytettäessä yhtä kuplakokoa, kaasun osuus reaktorissa sekä aineensiirtonopeus noudattavat toisen asteen polynomifunktiota. Sekoittimen tulvimispiste oli 9000m^3/h läheisyydessä ja aineensiirtonopeus tulvimispisteeseen eri kaasusyötöillä nousi 0.0394:stä 0.1074s^{-1}.

TABLE OF CONTENTS

Nomenclature

Roman symbols

a	interfacial area	m^2m^{-3}
C	impeller height	m
D	impeller diameter	m
d_B	bubble diameter	m
D_L	diffusivity for liquid	m^2s^{-1}
g	gravitational acceleration	ms^{-2}
G_B	generation of turbulence kinetic energy due to mean velocity gradients	m^2s^{-2}
G_k	generation of turbulence kinetic energy due to buoyancy	m^2s^{-2}
H_L	height of fluid level	m
H_T	height of tank	m
i	i^{th} component	
k	turbulence kinetic energy	m^2s^{-2}
k_L	mass transfer coefficient	ms^{-1}
k_La	mass transfer rate	s^{-1}
k_P	turbulence kinetic energy at point P	m^2s^{-2}
L	characteristic linear dimension	m
m	mass	kg
N	impeller rotational speed	s^{-1}
N_{js}	minimum impeller speed to just suspended solid particles in vessel	s^{-1}
P	power	W
Q	gas flow rate / pumping capacity	m^3s^{-1}
$\vec{R}$	drag force that is proportional to mean velocity difference	N
S_k	user-defined source term for turbulent kinetic energy	m^2s^{-2}
S_ϵ	user-defined source term for turbulent dissipation rate	m^2s^{-3}
T	tank diameter	m
t_c	circulation time	s
$t_{computation}$	simulation time	s
T_L	integral time scale	s
t_m	mixing time	s
T_Q	torque	Nm
U	mean velocity	m/s
U_i	velocity component	m/s
u'_i	fluctuating velocity component	m/s
U_P	mean velocity of fluid at point P	m/s
U_{slip}	slip velocity	m/s

U_T	particle terminal velocity	m/s
V	volume	m^3
v_s	superficial gas velocity	m/s
v_{tip}	tip speed of impeller	m/s
vvm	volume of gas flow per vessel volume per minute	min^{-1}
$\dot{\gamma}$	nominal shear rate in the rotor-stator gap	s^{-1}
Y_M	contribution of the fluctuating dilatation in compressible turbulence to the overall dissipation rate	m^2s^{-3}
y_P	distance from point P to nearest reactor wall	m

Greek symbols

α	volume fraction	-
β	thermal expansion coefficient	K^{-1}
δ	shear gap width	m
ε	turbulence energy dissipation rate	m^3s^{-3}
ε'	local turbulence energy dissipation rate	m^3s^{-3}
μ	dynamic viscosity	Pas
μ_{eff}	effective viscosity	Pas
v	kinematic viscosity	m^2s^{-1}
ρ	density	kgm^{-3}
σ	surface tension	Nm^{-1}
τ_B	relaxation time for bubble	s
τ_w	viscous shear stress near wall	Pa

Dimensionless numbers

C_D	drag coefficient
$E\ddot{o}$	Eötvös number
Fl_G	gas flow number
Fr	Froude number
K_{GL}	gas-liquid exchange coefficient
K_T	Metzner-Otto constant
N_P	impeller power number
Re	Reynolds number
Re_p	relative Reynolds number
Stk	Stokes number
κ	von Kármán constant
σ_k	turbulent Prandtl number for turbulence kinetic energy
σ_ϵ	turbulent Prandtl number for turbulence energy dissipation rate

Subscripts

G	Gas
I	Impeller
L	Liquid
S	Spinarea
T	Tank

Abbreviations

ARA	Arachidonic acid
B.C.	Boundary condition
BPC	Bioprocess container
CFB	Circulating fluidized bed / Steam reforming reactor
CFD	Computational fluid dynamics
DES	Detached eddy simulation
DFB	Dual fluidized bed
DME-SR	Dimethyl ether gas adsorptive separation and stream reforming
DNS	Direct numerical simulation
FCC	Fluid catalytic cracking
HTR	High temperature regenerator
IBC	Impeller boundary condition
LES	Large eddy simulation
MRF	Multiple reference frame
NRMSE	Normalized root mean square error
PIV	Particle image velocimetry
RDT	Single Rushton turbine
RNG	Re-normalization group
RSM	Reynolds stress model
SIMPLE	Semi-implicit method for pressure-linked equations
SM	Sliding mesh
SUT	Single-use-technology
UDF	User defined function
VOF	Volume of fluid

1   INTRODUCTION

Computational fluid dynamics (CFD) is a field of study where fluid behavior is calculated with mathematical methods. These methods are made either by using known physical and/or chemical equations, which are then improved and validated through the use of experimental data. In this study CFD was used to study behavior of gas-liquid mixing in an industrial scale draft tube reactor with different gas feeds. Gas-liquid mass transfer is usually the bottleneck for bioprocesses, especially in industrial scale, making it a target of interest.

CFD modeling tools are radically being developed and improved in terms of computational capability available and new physicochemical equations being introduced that are based on literature reviews and experimental data gathered for certain processes. These have improved and will improve testing of novel technologies beforehand in safe conditions with less time and investment costs than a high-quality experimental facility would require. In case of a new complex process, there should always be some kind of experimental setup, which can then be revised and improved by means of CFD. This study will go through the process of scaling-up laboratory size model to industrial size and simulating gas-liquid mixing by using procedures based on years of industrial experience.

1.1   Background

Multiphase flows are getting simulated more and more accurately in CFD based on the assumption that the equations/models used are suitable for the process setups. Multiphase flows include gas-liquid, liquid-liquid, liquid-solid and gas-liquid-solid systems that can be either in turbulent (stirred tanks) or laminar flow regimes (smooth fluid flow) as well as combinations of these two. This study has taken an interest in gas-liquid fermenting process that has tiny microbes (< 1μm), which do not affect water rheology and the solution can be treated as single phase.

Fermenting process takes place in a bioreactor, which is an engineered device that supports biologically active environment (McNaught 1997). Bioreactors may have issues with

stability and reaction rates, which is why they require solution to be homogeneous. In this study, a draft tube reactor has been proposed for improved circulation as it combines the radial distribution of fluids through mixing and enhances the axial circulation of fluids through the centrally located draft tube. The reactor in this case is commercial OKTOP®9000 reactor that is also designed for leaching processes. (Tervasmäki *et al.* 2016)

The fermentation reaction is mainly driven by gas-liquid interphase mass transfer, where gas is fed from the bottom of the reactor with ~30m/s discharge velocity. Gas hits the impeller and gets dispersed by the rotating blades, breaking into smaller bubbles. The draft tube itself enhances circulation in the reactor as there is a down current created inside the draft tube by the impeller. Microbes use the gas (e.g. carbon dioxide) to create ethanol. The process itself is continuous with fixed fluid level. The reactor is presented in Figure 1.
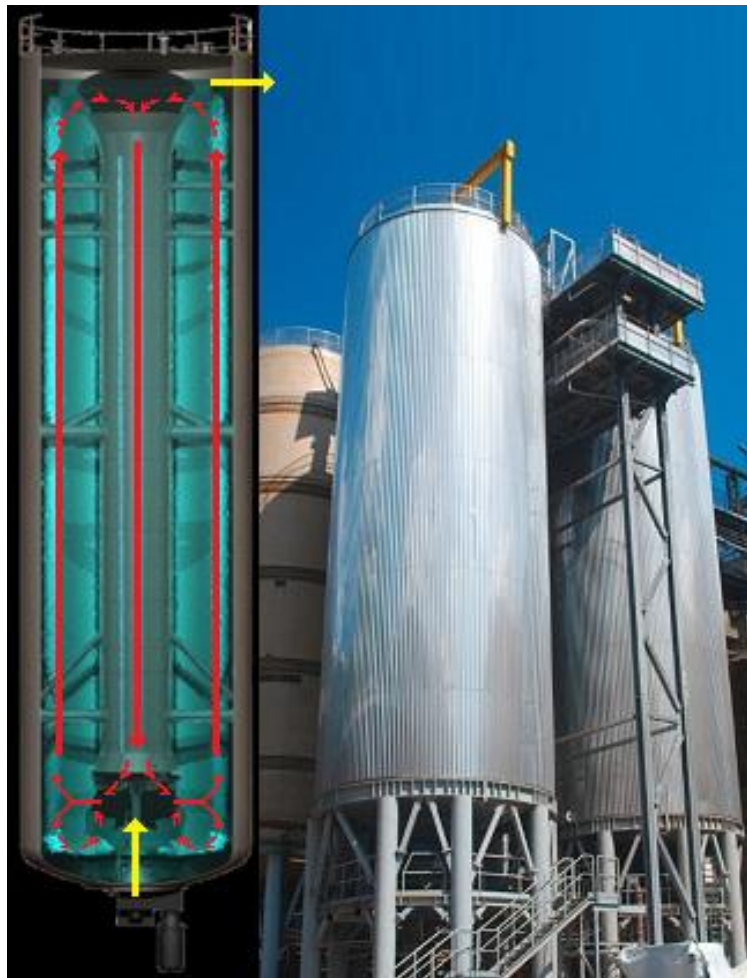

Figure 1. OKTOP®9000 Series reactor (Outotec). Main flow directions are indicated with red arrows. Feed flow and outlet flow are indicated with yellow arrows.

The main concern for microbial fermenting in a mixed reactor is that the mass transfer is affected by diffusivity, energy dissipation rate, gas void fraction and bubble size. Velocity of liquid affects mass transfer rate indirectly as higher velocity will yield higher energy dissipation rate. When it comes to terms of yields, traditional mixing tanks may give better results than a draft tube reactor, but at higher energy consumption. There was a mass transfer study in a cell cultivation and mixing made by Tervasmäki *et al.* (2016) on using draft tube reactor instead of traditional mixing tank that were validated with experimental data. The experiments were made in tap water and 0.03mol/L $MgSO_4$ solution as liquid medium (non-coalescing liquid and smaller bubble size). The authors came to a conclusion that the draft tube reactor achieved higher mass transfer rate than a standard three Rushton turbine stirred tank reactor with similar agitation power. Also the uniformity of dissolved gas was better in the agitated draft tube reactor.

1.2 Objective

In this study an industrial sized bioreactor was simulated. Gas-liquid mixing was simulated in a commercial agitated draft tube reactor, OKTOP®9000 ($985m^3$; width 7.5m; height 22.3m). The geometry of the reactor had previously been created in laboratory scale, which was scaled-up in this work to utility scale. The following modifications were added to improve simulation stability: raising the computational cell count (larger grid), refining the first grid cell size near walls and limiting the impeller spinning area to keep the width to height aspect ratio geometry of impeller due to scale-up similar to the laboratory scale. Euler-Euler per-phase model was used to simulate the gas-liquid process in steady-state. The phases that were considered in the simulation were water-ethanol 3% solution (continuous phase, liquid) and air (dispersed phase, gas). The surface tension used for the simulations was based on experimental data from laboratory scale (Bogatenko 2017). The assumptions for the simulations were the following:

- Non-coalescing system due to effect of ethanol (bubble breakage and coalescence were neglected in the models)
- The effect of hydrostatic pressure not considered (increases solubility of gas into liquid and decreases bubble size (Tsao 2014))
- Average bubble size of under 4mm, which can be considered as rigid particles

- Fluid height expansion is not considered as the process is continuous with a fixed fluid level
- Cell growth does not have effect in fluid rheology due to cell sizes of $< 1\text{-}5\mu m$ (Koch and Subramanian 2011)

Simulations based on laboratory size draft tube reactor had been made earlier related to FERMATRA project and they were in terms with the experimental data gained from study made by Tervasmäki *et al.* (2016). These simulations raised an interest in seeing how well CFD can predict the behavior of an industrial scale reactor. A utility scale simulation is the first of a kind for the mentioned process that the author is aware of and it will prove to be a good platform for improving industrial scale CFD simulations. The objectives of this study include:

- Performing study on drag laws that could be applied to the simulation process
- Making sensitivity analysis on the effect of bubble size
- Performing an analysis on the flooding point
- Performing an analysis on how gas feed affects the mass transfer
- Choosing a method for a utility scale simulation that can be achieved in realistic computational time ($t_{computation} \leq 1$ week)

The scaling-up has been performed through the use of a laboratory size geometry model, which has then been scaled to the industrial size dimensions. Thus reactor configuration is not exactly the same as industrial device. Even though there was a mesh independency test done to laboratory scale, a new test was required for the scale-up model as the volume of each cell increased roughly by a factor of 74000 (from 13.3L to 985m^3). There was also a rough estimation for the commercial reactor superficial gas velocity (v_s), tip speed of the impeller (v_{tip}) and impeller power number (N_P) available provided by Outotec.

In order to approach the given objectives, there has been a literature review on what kind of drag laws have been used on similar cases that are experimentally validated. When picking a suitable drag model, it had to be compared with the data acquired from the laboratory scale and similar experiments to see which represents the behavior of the process best. After this, a sensitivity analysis was made with the assumption that the

bubble size would vary from 3mm (± 1mm) to check the influence on gas-liquid mass transfer. The average bubble size was estimated from literature review.

The flooding point was analyzed by using correlation proposed by Nienow *et al.* (1985) where ratio of gassed-to-ungassed power is plotted against gas feed. The flooding under constant impeller speed will occur when there is a step jump in gassed-to-ungassed power. When this happens the impeller is overwhelmed by gaseous phase, which worsens gas dispersion. Simulation of the flooding point can be made with average bubble size as the volume around the mixing is highly turbulent and the bubbles are relatively small and therefore spherical.

Analysis on the mass transfer however may differ from the actual as the bubble size varies inside the reactor due to high mixing intensity (~ 1kW/kg) near the impeller vs. the vessel-average mixing intensity (~ 0.28kW/kg). Also, high hydrostatic pressure in the reactor can increase solubility of gas phase and decrease the bubble size which will increase the interfacial area to some extent, whereas the bubbles that rise from the bottom's higher pressure to the top's lower pressure expand (Tsao 2014).

As there is no available experimental data from industrial size reactor, the results and methods in use must be validated through the means of literature review with data on similar applications that are backed with laboratory sized experimental data. These will be used for comparison with acquired results. Industrial scale-up challenge will be the fact that keeping the same volume of gas flow per bioreactor volume per minute, *vvm*, while increasing the scale, the magnitude of the liquid velocity increases, but fails to match the mixing intensity observed in laboratory scale.

1.3 Scope of Work

The literature part of this thesis is covered in Chapters 2-6. Chapter 2 reviews CFD simulations regarding scale-up and general scaling-up procedures for different multiphase processes with the emphasis on agitated vessel, gas-liquid and bioreactor scaling-up that is studied in this work. There are also studies by different authors that are dealing with different kind of scaling-up procedures in Chapter 3. The simulation methods, objectives,

possible problems and the results that were obtained are also discussed in the chapter. After this (Chapters 4-6 respectively), there is a review on modeling geometry, meshing, the theory of physical phenomena that are considered to take place in this process and the boundary conditions that are used for the simulations.

The experimental part is presented in Chapters 7-9. It consists of investigating how different gas feeds affect 3 different main variables at constant impeller rotational speed: gas hold-up, mass transfer rate and gassed power draw. The bubble sensitivity analysis will present how the change in average bubble size would affect the simulation results. These are simulated with ANSYS Fluent 18.0, a commercial CFD-software. There will also be information on how the model's geometry was treated, what kind of problems were encountered during the simulations and how these were approached and dealt with. There are also further development ideas for OKTOP®9000 to be utilized in, that are presented in Chapter 10.

LITERATURE PART

2   CFD SIMULATIONS AND SCALE-UP

CFD can be used to broaden design correlations and experimental data. It can provide comprehensive data that cannot be easily obtained just from experimental tests in case the used methods are appropriate. CFD complements scale-up since the models are based either on fundamental physics (e.g. conservation of mass) and/or approximations (e.g. turbulence models) and are not bound to certain geometry or scale. Since CFD has been proven to predict fluid dynamics in laboratory scale reactors in previous FERMATRA studies with good accuracy, it is of interest to study how well it can be applied to multiphase mixing in actual operational units of industrial size. On top of that, CFD can be used in trouble-shooting to help finding the root cause of an operational unit failure. It facilitates to understand physical modeling better and improvements that can be made based on certain type of reactor and phenomena studied (e.g. drag force correlations). CFD also helps in understanding the real process better (e.g. when dealing with fluids that cannot be observed optically in petrochemical industry). There is also the possibility of creating many "what if" scenarios safely and analyzing them in less time and costs than it would take with experimental tests. (Marshall and Bakker 2004)

CFD simulations are often applied to laboratory or pilot plant size reactor in order to roughly figure out how fluids behave in an industrial scale reactor. However, there might be some phenomena in industrial scale setup that are absent from laboratory and pilot scale setups. These simulations usually have an experimental reactor in order to validate and raise confidence in the simulated results in comparison with the acquired experimental data. In case of an industrial size simulation where there is very limited or no experimental data of same scale to validate the simulation results, validation has to be made based on data acquired from laboratory/pilot size simulations, experimental data and research data on fluid behaviors in similar processes. If there are any experimental experiences or even scarce large scale experimental data available, those can also be used to judge the validity of large scale CFD results. (Etchells III and Meyer 2004)

Single phase flow is often pretty straightforward to simulate, however when more phases are introduced there will be many different factors that are hard to couple by mathematical means (e.g. simultaneous coalescence, dispersion, suspension, mass transfer and chemical reaction). Multiphase flows are also more often transient in nature than single phase flows. If a system is complex, then it is important to understand the goals of the process and to get proper data for all the components involved such as physical, chemical, and interfacial properties as well as reaction kinetics. After this, simulating a simplified version of full scale mixing process will help to visualize at least the flow pattern or even dispersion. From the acquired simulation data it is easier to identify where the main problems might occur in terms of coalescence, circulation time or settling. Once a CFD model has been properly designed and used settings validated, operating parameters and different scales can be compared to determine the sensitivities of design. CFD models of large scale require huge amount of elements, as the spatial discretization will get affected by scale-up of reactor volume, in order to get proper accuracy, leading to bigger computational costs. Compromises between accuracy and poorer spatial discretization need to be made to keep the computational time viable for industrial use. These statements conclude that a successful scale-up does not mean that identical results are obtained at two different scales, but rather, that the scale-up results are predictable and acceptable. (Leng and Calabrese 2004)

Even though simulations have proven to **(1)** cost less time- and equipment wise compared to experimental tests, they have not yet reached the point where the results could always replace experimental results. Surely, when more phenomena get correlated based on systems under study and physicochemical behaviors are explained better by mathematical means, simulations become more independent. However, at the moment simulations prove to **(2)** give many results in a relatively short time in case the process is generally known to user. **(3)** They give important data on details of flow, turbulence and/or mixing rate that cannot be experimentally studied conveniently. **(4)** Since simulations are based on fundamental physics and/or approximations, they are more likely to give potentially more realistic information on the performance of a process, rather than, the methods based on dimensional analysis, mechanistic approximations, or space-averaged theories or correlations. This however requires that the model equations in use are well defined and can be validated by comparison with the flow that has been observed in experimental

studies. **(5)** When simulating mixing effects in reactors, the initial data of the process has to be known. These include physical properties like viscosity, density, diffusivity and geometrical configuration of knowing where the mixer(s) and the feed(s) are located. **(6)** The biggest issue with simulations is the uncertainty of reactions that take place with more heterogeneous or homogeneous reactions in multiple phases. The momentum of phases needs to be coupled in order to catch the proper interaction between phases. However, the progress that CFD has made is significant as the literature from 2004 stated problems occurring with gas-liquid-systems (Patterson *et al.* 2004) and in less than 10 years, more and more correlations for different processes have arisen with reasonable results supported by experimental results.

Often, even if not always, it is not necessary to obtain exact results for industry. Engineering level of accuracy is sufficient in such cases. What is crucial, however, is that the model is able to predict trends and sensitivities correctly. This means that when, for instance, gas feed rate is changed, the model should be able to predict whether the situation gets worse or improves and also how sensitive the results are for the change.

2.1 General Scale-up Rules for Agitated Vessels

When reactor gets scaled-up, the mixer design must be adjusted to obtain similar process parameters. Scale-up criteria depends highly on what kind of process is being considered, and are there geometric similarities that can be used to designer's favor. These include ratios between impeller and tank diameter (D/T), clearance of impeller (C/T), location of inlets, baffles and the ratio between liquid height and tank diameter (H_L/T). In Figure 2, two commonly used scale-up criteria are demonstrated from which the left one is based on holding power per unit volume (P/V) and the right one on torque per unit volume (T_Q/V) are kept constant when scaling-up. Some vendors prefer to use T_Q/V criterion since it has a direct impact on the overall size and cost of mixer, including gearbox. The exponents, y and x, should be determined experimentally or verified for the processes listed in the plots. (Hemrajani and Tatterson 2004)

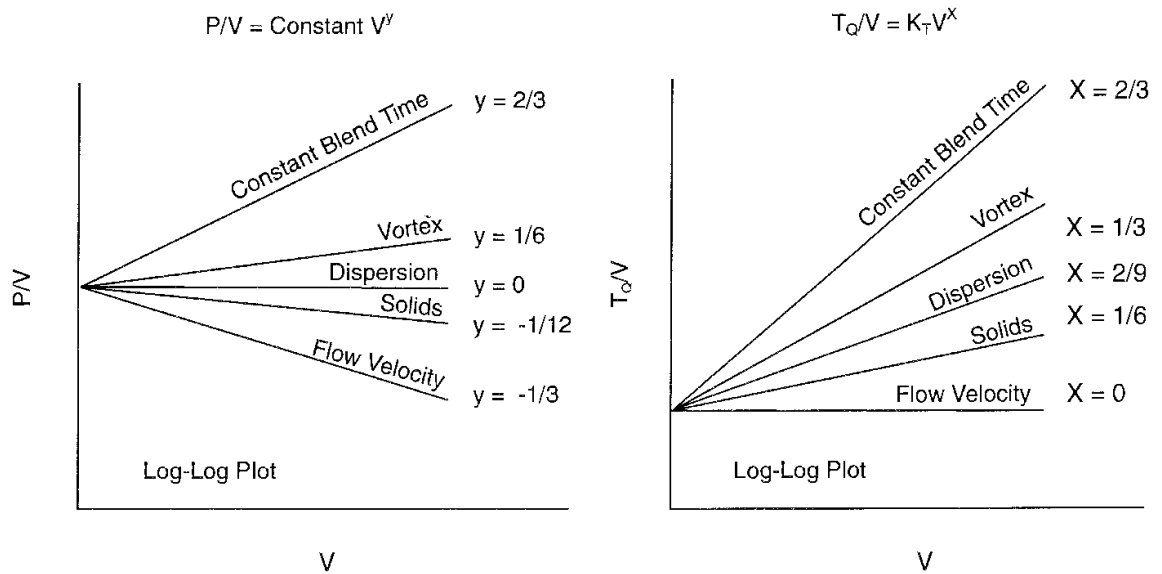$$P/V = \text{Constant } V^y \qquad\qquad T_Q/V = K_T V^X$$

Figure 2. Commonly used scale-up procedures for different process types and requirements. (Hemrajani and Tatterson 2004)

Vendors also often use equal rotor tip speed for designing and scaling-up rotor-stator mixers, where $v_{tip} = \pi ND$ (N is impeller rotational speed in RPS). Since majority of industrial rotor-stator mixers' shear gap width δ remains the same on scale-up, the tip speed criterion is equivalent to equal nominal shear rate in the rotor-stator gap ($\dot{\gamma} \sim v_{tip}$). (Atiemo-Obeng and Calabrese 2004) When scaling-up with constant P/V, the rotational speed and shear rate change significantly. Based on equations $\dot{\gamma} \sim v_{tip}$ and $\dot{\gamma} \sim K_T N$, where K_T is Metzner-Otto constant for shear rate vs. mixer speed; the maximum shear rate increases on scale-up while the average shear rate in the impeller region decreases (Metzner and Taylor 1960). The impact of scaling-up impeller is shown in Figure 3.
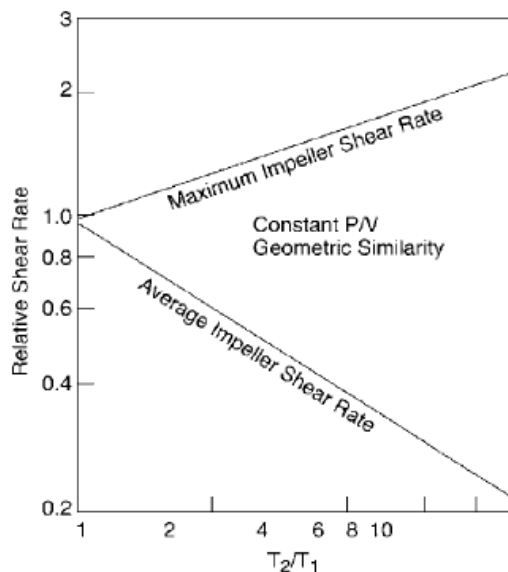

Figure 3. Impact of scale-up on impeller. (Hemrajani and Tatterson 2004)

Table I demonstrates how a scale-up to 10 times in diameter and 1000 times in volume of laboratory mixing tank behaves and what kind of importance there is in choosing a scale-up method as changes in other flow and power parameters have impact on the process results. If, for instance, the mixer rotational speed is kept constant (N=1) between laboratory size and commercial size, there is a huge increase in the motor power (P). This is usually applied to commercial reactors, which are relatively small in size and used if the reactions kinetics are from fast to instantaneous. When constant P/V (=1) is in use, the mixer speed decreases and the blending time increases. This means the scaled-up reactor may need to be sized to have longer residence time due to increase in blending time. (Hemrajani and Tatterson 2004)

Table I. Influence of scale-up by a factor of 10 in diameter and 1000 in volume on the most important changes in mixing parameters for geometrically similar systems (Hemrajani and Tatterson 2004)

Quantity	N	Q/V	Tip Speed	Re	T_Q/V	We	P/V	P
Changes in parameters	**1**	**1**	10	100	100	1000	100	10^5
	0.1	0.1	**1**	10	**1**	10	0.1	100
	0.22	0.22	2.2	21.5	4.8	48.4	**1**	1000

It should be noted that scale-up, based on local mixing conditions, is essential in case it is not possible to perform complete simulations of flow in vessel and perfect mixing or plug flow cannot be assumed. Especially, when observing mixing effects on yield with multiple reactions in stirred reactors that have geometric similarity and feed locations are in the most turbulent location scale-up should be approached simply by holding constant power per unit volume (P/V). If more precision is required, it is advised to hold the rate of turbulence energy dissipation per unit mass (ε/m) in the most intense mixing location constant as a scale-up criterion. This can be applied to processes where gas is fed into the impeller stream of a stirred vessel where mixing is the most intense, such as in this work. When studying geometrically similar mixing vessels, it should be noted that the local turbulence energy dissipation rate per unit mass (ε'/m) is proportional to the overall power per unit volume (P/V), so the two criteria should provide similar results. (Patterson *et al.* 2004)

In a case of heterogeneous reactions, new issues can surface when scaling-up. If a process is known to be driven mainly by mixing and there are organic reactions that have multiple

by-products, the ratio of other by-products formation should be maintained constant. If the by-products increase as little as 0.1%, it can be a significant problem. Thus product quality and downstream processing must not get worse than what the objective is, as this will determine whether the scale-up of process is a success or a failure. (Patterson *et al.* 2004) If there is no relevant data from the specific process, then extensive experience with similar processes can be applied. In case of a multiphase or fast reaction process: method selection, scale-up and design will be the main issues for mixing equipment. For such cases, it is necessary to perform several experiments at two or more different scales, where the vessel size based on diameter of vessel should get enlarged by at least a factor of 2. (Atiemo-Obeng *et al.* 2004)

Mass transfer dependent reactions involving coalescence and dispersion, such as this case, have a "rule of thumb" of scaling based on ND^X=constant. This is based on years of industrial experience and in order to apply it, Reynolds number has to be greater than 104 and vessels must have geometric similarities. Table II explains the scaling process depending on process application and which parameters or ratios are kept constant. (Leng and Calabrese 2004)

Table II.   Rule of thumb for scale-up of geometrically similar vessels at turbulent conditions based on ND^X = constant (Leng and Calabrese 2004)

Value of X	Rule	Process Application
1.0	Constant tip speed, constant T_Q/V	Same maximum shear; simple blending; shear controlled drop-size
0.85	Off-bottom solids suspension	Used in Zwietering equation for *N_{js} for easily suspended solids; also applies to drop suspension.
0.75	Conditions for average suspension	Used for applications of average suspension difficulty.
0.67	Constant P/V	Used for turbulent drop dispersion; fast settling solids; reactions requiring micromixing; gas-liquid applications at constant mass transfer rate.
0.5	Constant Reynolds number	Similar heat transfer from jacket walls; equal viscous/inertial forces.
0	Constant speed	Equal mixing time; fast/competing reactions.

*Minimum impeller speed to just suspended solid particles in vessel (RPS)

It can be noticed from Table II that most of the scale-up rules apply for suspension, dispersion, heat transfer and reaction rates of different levels. This is why it is important to identify the phenomenon that affects or limits system the most and focus on that.

Table III presents further how scale-up affects geometrically similar systems. If power per unit volume (P/V) is used, then it will result in a lower impeller rotational speed (N), higher tip speed (v_{tip}), pumping capacity (Q), mass transfer k_La (at constant vvm), and circulation time (t_c). When one parameter is kept constant other important variables will change. Therefore, the choice of scale-up rule is not set in stone given the potentially sensitive and diverse responses of cells to each of the forces influenced by impeller design, system geometry, scale, fluid properties and operating parameters. (Amanullah *et al.* 2004)

Table III. Different scale-up criteria and their effect when applying a linear scale-up factor of 10 and maintaining geometrical similarity ($Re > 10^4$) (Amanullah *et al.* 2004)

Large Scale/ Small Scale Value	Equal P/V	Equal N	Equal v_{tip}	Equal Re	Equal k_La and vvm	Equal k_La and v_s
			Scale-up Criteria			
$P \sim N^3D^5$	1000	10^5	100	0.1	829	1000
$P/V \sim N^3D^2$	**1**	100	0.1	10^{-4}	0.8	**1**
N or t_m^{-1}	0.22	**1**	0.1	0.01	0.3	0.22
$v_{tip} \sim ND$	2.2	10	**1**	0.1	2.7	2.2
$Re \sim ND^2$	22	100	10	**1**	27.2	22
$Q \sim ND^3$	220	1000	100	10	272	220
*$Fr \sim N^2D$	0.48	10	0.1	10^{-3}	0.5	0.48
$t_c \sim N^{-1}$	4.55	**1**	10	100	9.4	4.55
k_La at equal vvm	1.59	39.8	0.32	$2.5 \cdot 10^{-5}$	**1**	--
k_La at equal *v_s	**1**	25.1	0.2	$1.6 \cdot 10^{-3}$	--	**1**

*Froude number (6.1 Impeller for more information)

Regardless the choice of scale-up criterion, there is always an increase in circulation time (t_c) at large scale. This does not apply to scaling-up with equal impeller rotational speed (N) or mixing time (t_m), however they are not economically feasible as the power consumption rises. (Oldshue 1966; van't Riet 1979) Increased circulation may have an effect on mass transfer in case of a gas-liquid system due to passive gases, such as nitrogen, that are mixed in with oxygen. As soon as oxygen is transferred from a bubble, only nitrogen is left behind, which does not contribute to mass transfer. (Calderbank 1959)

2.2 Solid-Liquid Scale-up

When the application is solid-liquid-based, the purpose of scale-up is to determine what kind of operation conditions at different scales are in order to receive satisfactory mixing yields equivalent process results. This requires (**1**) definitions for appropriate desired process results (e.g. uniformity of solid distribution or rate of reaction between solid and liquid reactants), (**2**) developing reliable correlations that describe behavior of a system by either experimentation or mathematical analysis of a physicochemical phenomenon taking place, (**3**) validating the results for key controlling physicochemical phenomena and (**4**) applying those correlations to predict process performance at different scales. (Atiemo-Obeng *et al.* 2004)

2.3 Liquid-Liquid Scale-up

In case of immiscible liquid-liquid scale-up it is important to identify applications by types likely to cause problems and focus more on those, rather than, more trivial applications that hardly affect the overall behavior of a system. Good example for this is a mixing tank where mixing plays the most critical part. Successfully scaled operations are fully anticipated and understood. The performance of the operation is usually poorer than witnessed on a smaller scale since the gradients with larger scale will have bigger impact on the behavior of the operation (e.g. hydrostatic pressure increase with height increase, difference in force brought by larger mass or exothermic reactions). This phenomenon can be witnessed in liquid-liquid as well as in gas-liquid systems as smaller scale systems tend to be dominated by dispersion whereas industrial scale ones by coalescence. The cause for the mentioned phenomenon is mixing intensity and high shear rate in small scale (intense) vs. large scale (gentle) and also physicochemical interactions between fluids (e.g. bubble size in water-gas varying vs. water-ethanol-gas being more uniform). The errors that occur due to improper scaling can lead to losses in capacity, quality, safety, and therefore profits. (Leng and Calabrese 2004)

If a system, however, is highly coalescing, there is no exact method to assure successful scale-up. When such system is under observation, it is (**1**) a question of whether the process requires coalescing or non-coalescing conditions, (**2**) can the coalescence rate be

characterized by using either static or dynamic method and, if needed, reduce the coalescence and **(3)** is there a possibility to enhance recirculation of fluid and/or dispersion of liquid (also gas) by introducing more mixers or by other means. The guidelines for scaling-up such liquid-liquid (and to some extent gas-liquid) stirred vessels are presented in Table IV. (Leng and Calabrese 2004)

Table IV. Guidelines for general purpose liquid-liquid agitated vessels scale-up (Leng and Calabrese 2004)

Feature	Non/Slowly Coalescing System	Rapidly Coalescing System
Scale-up criterion	P/V = Constant	Circulation time = Constant
Scale-up limitation, V_{Large}/V_{Small}	100 : 1	10 : 1 to 20 : 1
Baffles	Yes (not for suspension polymerization!)	Yes
Impellers	*RDT and optional axial flow/hydrofoil impeller	Multiple RDTs and axial flow/hydrofoil impeller for better circulation
D/T	0.3 - 0.5	≥ 0.5
Time to reach terminal drop size	Long times for large vessels	Short times under 30 min for most coalescing systems (all vessel sizes)
Geometric similarity	Maintain close similarity	Use more and larger turbines in larger vessel; do not try to maintain geometric similarity
Speed/drives	Variable or fixed speed	Variable speed capability is essential; consider overdesign to meet unpredicted performance
Risk	Low to moderate risk	High risk

*Single Rushton impeller

2.4 Gas-Liquid Scale-up

There are a lot of good literature articles that strengthen the fact how the relation between gas flow energy and mixer energy work out. These include Nagata (1975), Oldshue (1983) and Smith (1985). When studying a mixing reactor with radial flow impeller, the mixer energy must be around three times greater than the energy introduced by a gas stream that is fed towards the impeller. This ensures that the mixer will control the flow pattern.

(Oldshue 1983) Successfully scaling-up gas-liquid systems depends on the extent to which small scale vs. large scale characteristics resemble each other (Amanullah *et al.* 2004). When performing a scale-up, it is necessary to make a choice of method appropriate for the system even if other factors might get affected in different ways. Therefore, priorities have to be chosen since there is often no way of scaling all significant factors together as can be seen in Table III. (Middleton and Smith 2004)

Sometimes there are situations where geometric aspects are not similar between scaled-up and smaller vessel. In this kind of scenario scaling can be done based either on holding power per unit volume (*P/V*), *vvm* or tip speed $v_{2,tip}/v_{1,tip}=(D_2/D_1)^{(1/3)}$. In case of assuming that the power number (N_P) is scale independent and flow regime is turbulent, $N_2/N_1=(D_1/D_2)^{(2/3)}$ can be used for scaling. (Treybal 1966) This was agreed on by Skelland and Ramsey (1987) with a slight correlation of 0.71 to the exponent considering the gas hold-up in the system was low. If fluid properties or rate of constants are unknown, especially when mass transfer rate or dispersion is not known, experimental laboratory or pilot scale testing is required for simulations.

2.5 Bioreactor Scale-up Rules

When bioprocesses are in concern, like in this study, the most frequent problem is non-ideal or even unknown fluid flow behavior at large scale. Usually when mixing is studied in laboratory scale, the mixing itself is intense and uniform enough to effectively turn flow homogenous. When reactor dimensions are increased, circulation times will also increase and microenvironment experienced by a cell becomes a function of bulk flow, mixing and turbulence. This kind of behavior is difficult to predict. That is why it is important to focus on major points that have the biggest impact on reaction such as pH, substrate, dissolved oxygen, temperature or dissolved carbon dioxide that are responsible in performance differences at large scale. Scale-down models however can be used more effectively to understand causes and effects of a nonhomogeneous microenvironment on cell metabolism and optimize a process through the procedure. (Amanullah *et al.* 2004)

There are many methods of scale-up of aerated, stirred fermenters that follow certain criteria proposed by Hempel and Dziallas (1999) that include (**1**) equal specific energy

dissipation rates, **(2)** maintaining geometric similarity, **(3)** equal impeller tip speeds, **(4)** constant mixing times, **(5)** equal volumetric mass transfer coefficients, **(6)** equal oxygen transfer rates, **(7)** extrapolations or interpolations of test data generally secured for two scales and **(8)** combination of more than one of the criteria mentioned.

Oosterhuis and Kossen (1984) proposed one way to solve the problem of scale-up of bioreactors that is shown in Figure 4. First, a production scale is modeled in laboratory scale by scaling-down a reactor based on transfer rate-limiting parameter. After this, bottlenecking features can be optimized to enhance the process and be applied to production scale. The most important reason for scale-down is however to make it representative for the conditions at large scale.
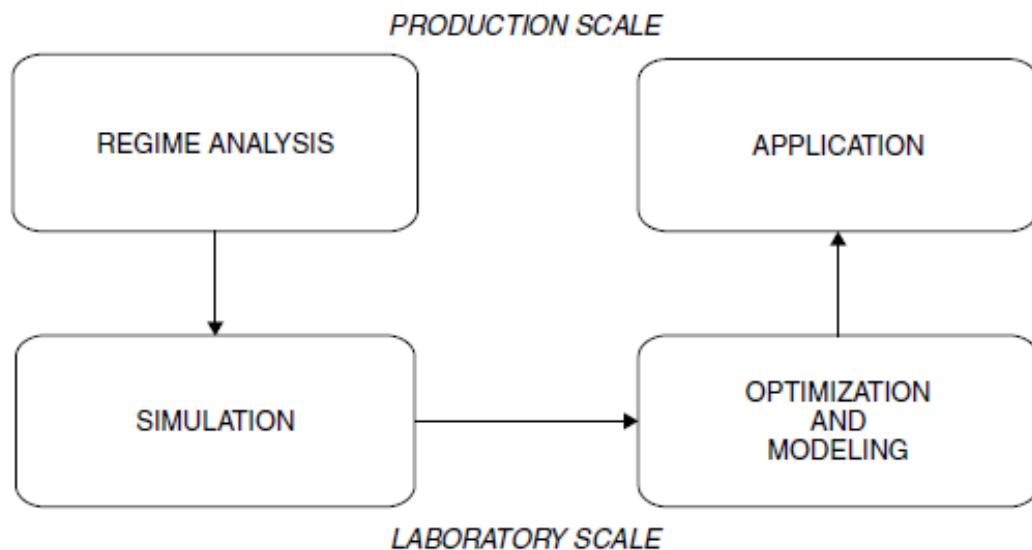

Figure 4.   Scaling procedure of Oosterhuis and Kossen 1984.

3   SCALING OF DIFFERENT APPLICATIONS

The main objective of scale-up in CFD is to validate models made in laboratory scale that can be used in large scale modeling with high enough confidence. There are parameters that need to be accounted in scaling procedure for as volume is increased. In this chapter, there is a compilation of 6 (A-F) different CFD modeling cases from literature that are all related to scale-up simulations in some way. This chapter will introduce what kind of methods were used, problems have arisen from the scale-up and what have been achieved as results in the studies. In the end of this chapter, there is a summary where Table VI and

VII present the CFD-software, mesh, methods and settings that were used in the simulations, whereas Table VIII shows what were the objectives, how the results were validated and what kind of problems were encountered.

3.1 Case A (Cubic Geometry Single-use-technology Bioreactor)

In case of bioreactors, there was a study made on a cubic geometry single-use-technology (SUT) bioreactor as a tool for the design process. The purpose of SUT is to reduce the time required to make different products in between batches with a low-cost reactor by cutting down the batch time from industrial scale of 8-10h to 1-2h. The vessels studied were 1000L and 200L of volumes, from which 1000L was an existing vessel and 200L was a proposed design for improving the mass transfer. The vessels had a disposable magnetically-driven impeller located centrally on the bottom of the vessel, which was modeled with the multiple reference frame (MRF) method, and two rings of 14 spargers located around the centrally mounted impeller. The tank geometry was decided to be kept non-cylindrical in order to make the platform more appealing to wider industrial biotechnology applications in terms of cost and simplicity. Benefit of symmetrical geometry is also the fact that the computational expense can be halved as the studied volume can be split. The geometry is presented in Figure 5.
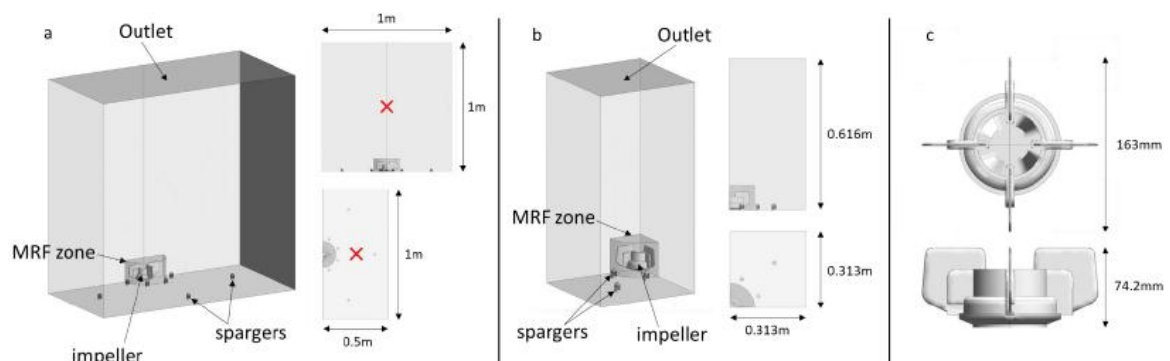

Figure 5. Geometry used to study SUT bioreactor. Computational time can be reduces with symmetrical geometry of the reactor. (Maltby *et al.* 2016)

The mesh used for both simulations was fully unstructured tetrahedral mesh due to complexity of MRF region geometry. Simulations were performed with ANSYS CFX-15. There were two phases considered for the Euler-Euler multiphase simulation: water as continuous and air as dispersed phase at 25°C. Bubble size was kept constant at 1mm

diameter. Degassing boundary was used for the outlet. The gas flow rates for inlets varied from 0.0675 to 0.1*vvm* and impeller rotation speeds from 100 to 500RPM. In the simulation heat transfer was not considered and the solver used was transient density-based solver as buoyance was modeled based on the density difference between two fluids. Turbulence was modeled with standard *k-ε* model with Schiller-Naumann drag model and additional drag force correlation, which represents the force exerted by the relative motion of the two fluids.

The main focus of the study was to simulate mass transfer k_La with five different models: penetration, slip velocity, eddy cell, rigid and surface renewal stretch model and find out which describes mass transfer the best. These models were defined by the author. The scaling of the vessels was done by keeping the aeration rate of the vessel (*vvm*) constant. The conclusion was that four out of those five models (eddy cell, penetration, rigid and surface renewal stretch models) gave reasonably consistent values of 2 to $40h^{-1}$ when compared with the limited experimental data available. The most suitable model to describe mass transfer in the mentioned process was the eddy cell model as it also presented the 'worst case' value for design purposes. (Maltby *et al.* 2016)

3.2   Case B (Internal-loop Airlift Reactors)

There was purely mathematical study done on internal-loop airlift reactors hydrodynamics with both, 2D and 3D model in Lappeenranta University of Technology (LUT), department of mathematics and physics. The used software for the CFD-study was ANSYS Fluent 12.1. The geometry for the airlift reactor was quite simple and symmetrical so the results from 2D and 3D had a very good agreement with each other. The system consisted of 3 velocity inlets at the bottom of the reactor and a pressure outlet on the top. Mesh also was quite coarse as it was refined from 390 cells to 24k cells in 2D (structured quadrilateral) and 780 to 19k cells in 3D (structured hexahedral). The geometry and mesh for the reactor are shown in Figure 6.

In the first simulation, set two phases were considered: water as continuous and air as dispersed phase and for the second simulation set solids were introduced into the fluid, however that will not be discussed in this section. Bubble diameter was constant 1mm. The

simulations used Euler-Euler multiphase with standard k-ε, mixture model for the 2-phase study with 1st discretization order. Those were solved by using a transient pressure-based solver. The simulations were initialized with 0.5% gas hold-up to get better stability in convergence.
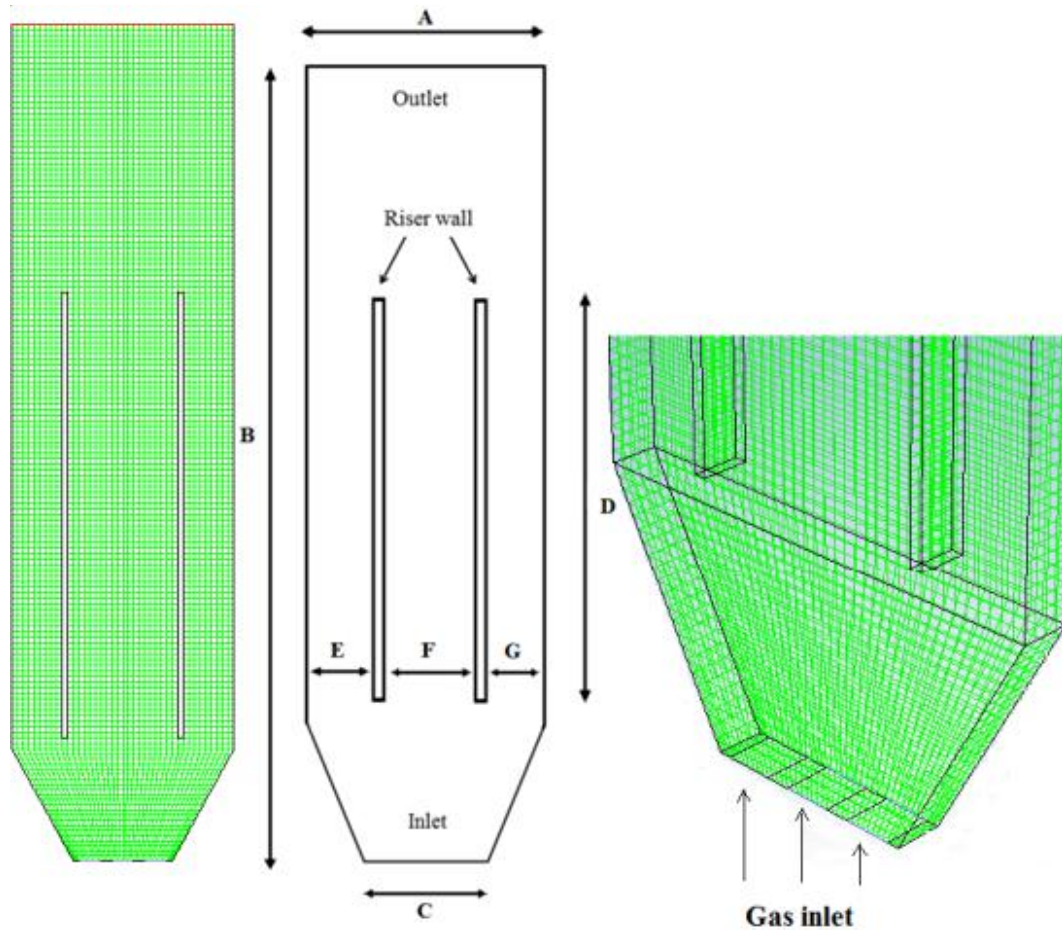

Figure 6. Internal-loop airlift reactor geometry and mesh to study hydrodynamics of gas-liquid system. (Patel 2010)

The target of the study was to see how grid refinement, time step, scaling of interiors would affect the hydrodynamics of the system. Grid refinement had more significance in 3D case than it did with 2D and the velocity got captured better with finer grid and the behavior of gas hold-up profiles became more parabolic. Time-step size (0.001 to 0.1s) however had only effect on liquid velocity. The geometry of the reactor itself has a significant impact on the change of the hydrodynamics parameter, which had been studied with 3 different settings that changed the internal structure of the geometry. The height of the reactor, B, width of the bottom, C, and the height of the riser tube D were kept constant during the scaling procedure. When the scale of the width, A, was changed larger it

reduced the friction losses with the angle between the bottom and the wall getting bigger and caused circulation of the fluid to increase. The enlargement in the downcomer (ExD & GxD) area increased the mixing of the gas and liquid. These features however decreased the overall gas hold-up. Scaling-down the downcomer area had reverse results. (Patel 2010)

3.3 Case C (Wastewater Treatment Plant)

In LUT Energy Technology department, there was a scale-up study made on a more complex geometry of part of a wastewater treatment plant that is referred as the mixing tank. Total volume of the geometry studied that is shown in Figure 7 was $363m^3$. Based on mesh independency it was decided to use medium quality mesh of almost 4M cells, which showed hardly any difference to fine mesh of 10M cells. The mesh in the pipes was O-type structured mesh whereas the mixing tank had multiblock structured-unstructured hybrid mesh applied to it. The system consisted of 3 inlets (2 in Duct from primary settling tank and 1 in By-pass pipe) and 4 outflow boundaries (Pipe 1 to 4).
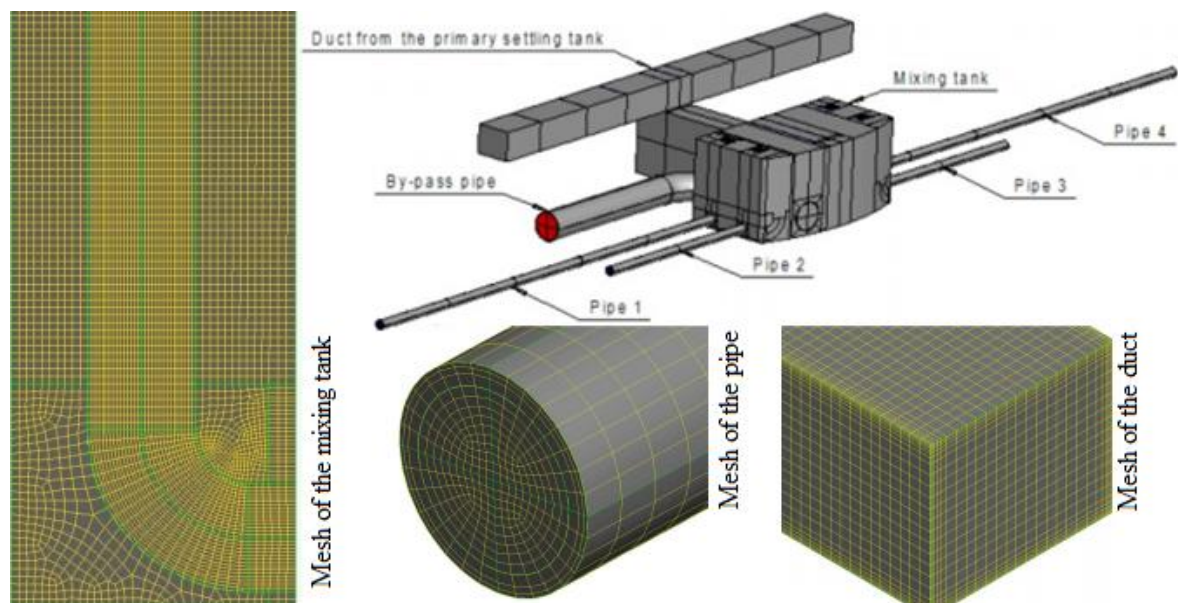

Figure 7.   The complex geometry of wastewater treatment plant and mesh. (Tiainen 2014)

The objective of the study was to study mixing phenomenon and how the solid particles spread in a wastewater treatment process and what were the effects of secondary flows on particles. The simulations were done by comparing steady-state results from mixture, drift-

flux and Euler-Euler model results using ANSYS Fluent 14.5. In case of the Euler-Euler model, outflow boundaries were not good for convergence and had to be changed into pressure outlets based on the data got from mixture models (static pressure). It was also mentioned that coupled algorithm improved the rate of convergence for the simulations. These were then analyzed in order to see the effect of changes in dispersed phase on flow regime and how the change in flow regime affects the modeling.

Since there was no experimental data available for comparison, the method to approach this case was to use average values based on literature: temperature (10°C), particle size (3.75mm), settlement values for concentration (102.5mg/L) and wastewater (315mg/L). The range for suspended solids' density was 950 to 1075kg/m^3 so the particles did not have any effect on the continuous phase as the volume fraction of the dispersed phase was below 1%. Different turbulence models were compared in the study and the most promising predictions could be acquired with realizable k-ε and SST k-ω models. Out of these two, realizable k-ε model took less computational time so it was chosen. For turbulent dispersion, an additional model by Burns *et al.* (2004) was used to see how it affects the results as it had a wide-range of universality and it had been validated for gas-liquid and liquid-solid flows in laboratory scale. The main issue with the simulations was the lack of experimental data, which made validation of the results hard. It was also noted that the flow regimes need to be known before starting simulations. (Tiainen 2014)

3.4 Case D (High Temperature Fluid Catalytic Cracking Regenerator)

An industrial size fluid catalytic cracking (FCC) high temperature regenerator (HTR) was studied in National University of Columbia-Sede. The height of the geometry was 22m and diameter 3.2m (V=~175m^3). The FCC regenerator consisted of a chamber, air distributor, catalyst inlets, combustor, regenerator vessel and 7 pairs of two stage cyclones. The geometry and mesh are presented in Figure 8. As this was first of the kind study, mesh independence was made for both, combustor design and regenerator design. For the combustor design, it showed that between 420k, 580k and 850k cell number meshes, 580k and 850k results varied so little, that in order to decrease the computational effort, 580k was used. The regenerator vessel was more complex and had meshes of size 1.5M and 2.2M, however the results were similar and 1.5M was used.
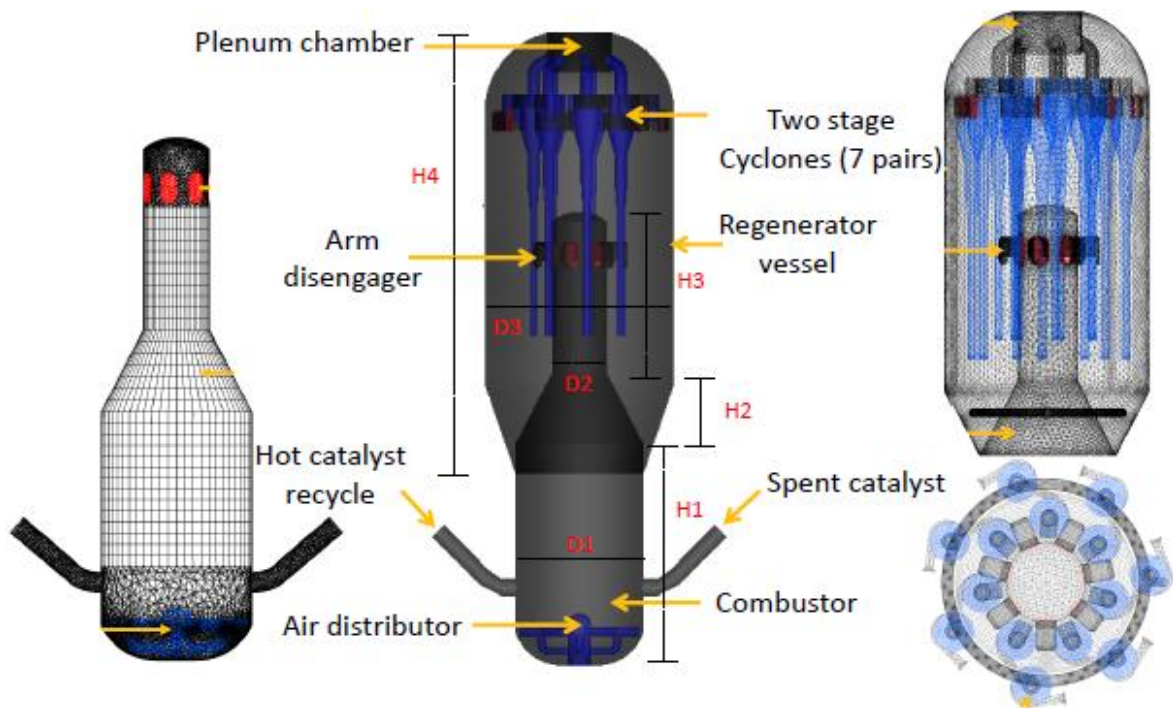
Figure 8.   Fluid catalytic cracking high temperature regenerator. (Alzate-Hernandez 2016)

The process was simulated with ANSYS Fluent 15.0. For the simulations, Euler-Euler granular flow model was used with a pressure-based transient solver that had 0.01s time-step size. Kinetics were solved with 1st order discretization and the maximum volume fraction for solid was set to 0.6. The particles were treated as effective particle clusters of 200 to 400μm with a density of 1500kg/m^3. Phenomena inside the FCC regenerator are complex and this increased the difficulty of predicting its performance. Therefore, drag force modification due to turbulence proposed by Li *et al.* (2009), which is based on different void fractions, was used as it showed satisfactory agreement between prediction and the experimental results. For the heat transfer, Gunn model was used. The operational conditions used for the simulations were mostly average values found from literature.

The objective of the study was to improve the performance of the FCC regenerator with a new design of introducing solids into the system. It was noticed that 2 simple inlets in the original design were not enough to guarantee proper radial solid distribution, but with six lateral and one central inlet in the new design showed a better distribution. There was also a suggestion to improve the transition of solids from the combustor to the regenerator vessel by changing geometry of the arm disengagers. (Alzate-Hernandez 2016)

3.5 Case E (Circulating Fluidized Bed Reactor)

In Aston University, there was a study on using CFD (ANSYS Fluent 14.5) in order to simulate industrial size dimethyl ether gas adsorptive separation and steam reforming (DME-SR) in a large scale circulating fluidized bed reactor, which was in this case proposed as a dual fluidized bed (DFB). This study as well as the previous case can be considered as battling a problem that had been noticed. In the current process the wanted product was silicone and unwanted product was dimethyl ether that needed to be removed. Euler-Euler dispersed model was used for this case instead of Euler-Lagrange as the latter took more computational time due to huge number of particles to track (Zhang and Chen 2007). It was mentioned, however, that by using Euler-Lagrange model a more detailed understanding of the absorbent particle characteristics and behavior would probably be accomplished. Syamlal-O'Brien drag model was chosen for the study as it predicts the behavior of fluidized bed systems satisfactorily according to the literature review. There were also two user-defined functions (UDF) made to model adsorption and DME-SR reaction. The solver used for this case was pressure-based phase coupled semi-implicit method for pressure linked equations (PC-SIMPLE) with granular flow. Pseudo first order with the time-step of 0.001s was used using the data from experimental work related to the same reactor.

The geometry of the simulations consisted of two parts, a bubbling bed and a steam reforming reactor (CFB), with diameter of 3m and height of 15m for both (V=106m^3), which are shown in Figure 9. The cyclones and catalyst regenerator were neglected from the study as they were not the main focus. The outlet of the reactors is set as pressure outlet and inlets were all set as mass flow except for bubbling bed, which was set as velocity inlet. The selected mesh size for the study was unstructured tetrahedral mesh of 117k cells for both CFB and bubbling bed simulations through mesh independence test as it had insignificant change in the results with 211k and 400k cells. 1.8M cells would have given even more accurate predictions, but the computational time for over 400k cells was too long so it got scrapped.
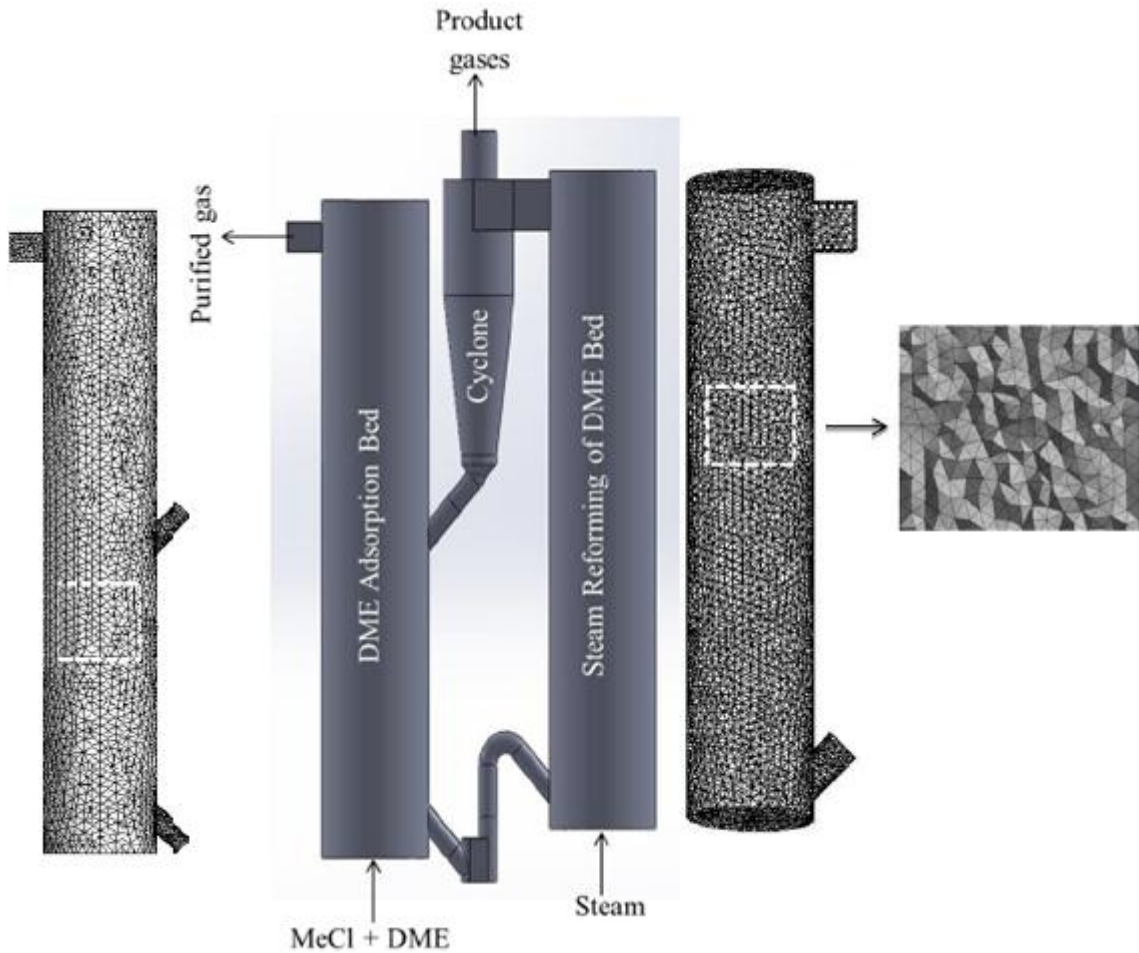
Figure 9. Circulating dual fluidized bed reactor. (Elewuwa 2016)

The superficial velocity of gas in bubble bed reactor was 0.48m/s and adsorbent (Mol4A) flow rate 20kg/s that had a particle size of 350μm and density of 720kg/m^3 in 25°C.For the DME-SR, steam of 300°C was fed with a flow rate of 5.86kg/s and DME of same temperature at 3.0kg/s with the addition of 2 catalysts of 150μm particle size with densities of 720 and 1300kg/m^3. These catalysts were fed with mass flow rate of 100kg/s each.

The conclusion of the study noted that over 88% of DME could be removed depending on the process conditions with at least 99% being the objective. The proposed model itself however showed good promise and with modifications could be brought to having even better efficiency. It should also be noted that this was the first simulation of DME-SR in large scale fluidized bed system. The main issue in the study was the lack of any experimental work, even in laboratory scale, which would have helped to validate the kinetic models in use. (Elewuwa 2016)

3.6 Case F (Industrial Gas-liquid-solid Stirred Reactors)

Similar to this work, there was a study made on two industrial gas-liquid-solid stirred reactors (with 3 multi-blade propellers) using MRF model, one being a scaled-up version of the other. The reacting volume itself however was composed of boiling liquid, solid and gas (bubble size of 1mm) and the reaction itself exothermic reaction (4/5 of the gas flow rate). This was also done with a different CFD-software, STAR-CD 3.2. The liquid-solid was treated as pseudo-liquid phase with the density of 642kg/m^3, dynamic viscosity (μ) of 9.83 · 10^{-4}Pas and surface tension (σ) of 0.00181N/m whereas the gas had density of 48kg/m^3 and dynamic viscosity of 1 · 10^{-5}Pas.

The inlet was a velocity inlet and the outlet was treated as a degassing outlet. Mesh (Reactor A 179k and Reactor B 233k cells) was structured hexahedral mesh except for the MRF areas which were unstructured due to complex impeller geometry. Reactor B volume was 1.86 times the volume of reactor A. From the profile data points and the images it can be deducted that the approximate diameter of the reactor is around 4.8 to 5.0m and from the ratio of the vessel the height is around 8.3m ($V=\sim160$m^3). The scaling-up procedure itself had to take into account different scaling methods for different parts as the reaction rate was quite fast and exothermic. The scaling procedure is presented in Table V.

Table V.   Geometrical and mixing characteristics of the reactors (Gentric *et al.* 2004)

Factor	Reactor A	Reactor B
Reacting volume V	V_A	$1.86V_A$
H_L/T	$(H_L/T)_A$	$0.955(H_L/T)_A$
$D_1/T = D_2/T$	$(D_1/T)_A$	$1.015(D_1/T)_A$
D_3/T	$(D_3/T)_A$	$1.20(D_3/T)_A$
*C_3/T	$(C_3/T)_A$	$(C_3/T)_A$
$(C_3-C_2)/T$	$[(C_3-C_2)/T]_A$	$1.025[(C_3-C_2)/T]_A$
$(C_2-C_1)/T$	$[(C_2-C_1)/T]_A$	$1.02[(C_2-C_1)/T]_A$
Rotation speed N	N_A	$0.8N_A$
Propeller tip speed	$v_{tip,1A} = v_{tip,2A}$	$v_{tip,1B} = v_{tip,2B} = v_{tip,1A}$
Turbine tip speed	$v_{tip,3A}$	$1.20v_{tip,3A}$
$N_{P1} = N_{P2}$	0.26	0.46
*$N_{QP1} = N_{QP2}$	0.49	0.66
N_{P3}	2.2	2.2
N_{QP3}	0.53	0.53
Specific power P/V	P_A/V_A	$2.23P_A/V_A$

*C is impeller height, N_{QP} is pumping number and 1, 2 & 3 are different impellers in the reactor

The results from the simulations were divided into three steps. First, the primary phase flows were compared between the tanks with the liquid-solid mixture being treated as a pseudo-liquid phase. After this, Euler-Euler simulations were done to investigate the two-phase flow gas distribution and finally injection of the killing gas had been simulated using a Lagrangian approach in order to see movement of 400 bubbles. The killing gas is a mean for plants to stop a chemical reaction from occurring and for this purpose the dispersion of the gas was a target of interest. In this case standard k-ε model was used to simulate turbulence. Wang correlation, which is derived from experimental data on single bubbles rising in water, was used to describe the dependence of C_D on bubble Reynolds number (Wang and Stock 1993). MRF and sliding mesh (SM) were both applied to impellers and the results compared with each other.

The conclusion of the study was that SM and MRF techniques gave similar results for the velocity when time-averaging the SM calculated velocities. Power numbers that were calculated using the torque of the pressure and shear forces on the impeller blades agreed with ones given by the manufacturer. Standard k-ε model however underestimated the dissipated power. This was noticed especially in the gas-liquid-solid flow simulation, where bubble velocity was low compared to the velocity induced by the impellers and the flow field was close to the single-phase one. The injection of the killing gas was noticed to be problematic for Reactor A as it did not disperse the gas properly, whereas Reactor B with larger bottom turbine dispersed the killing gas better. After either enlarging the size of the bottom turbine or changing the injection position, Reactor A had a better gas dispersion. (Gentric *et al.* 2004)

3.7 Compiled Information of the Simulations

All of the simulations, with the exception of just studying how hydrodynamics behave in CFD (Case B), had similar problems with validation of scale-up results. This could be seen especially in the complex geometry of Case C with the lack of experimental data. Table VI and VII present the summary of the used software, CFD methods and model set-up. Table VIII will show what were the objectives for each case, how the results were validated and what kind of problems were encountered.

Table VI.   CFD-Software, mesh and methods used in the mentioned CFD simulation cases

Case	CFD-Software	Grid size	Particle/Bubble size	Steady/Dynamic
A	ANSYS CFX-15	N/A	1mm	Dynamic
B	ANSYS Fluent 12.1	2D: 390 – 24k 3D: 780 – 19k	1mm	Dynamic
C	ANSYS Fluent 14.5	~4M	3.75mm	Steady
D	ANSYS Fluent 15.0	Combustor: 580k Regenerator: 1.5M	200 - 400μm	Dynamic
E	ANSYS Fluent 14.5	CFB: 117k	150 - 350μm	Dynamic
F	STAR-CD 3.2	Reactor A: 179k Reactor B: 233k	1mm	Dynamic

Table VII.   Methods that were used in the mentioned CFD simulation cases

Case	Turbulance model	Drag model	Additional models	Phases
A	Euler-Euler, standard k-ε model	Schiller-Naumann	Drag force correlation	Gas-Liquid
B	Euler-Euler mixture, standard k-ε model	Schiller-Naumann	-	Gas-Liquid
C	Euler-Euler mixture, dispersed and per-phase, realizable k-ε model	Schiller-Naumann	Turbulent dispersion model (Burns *et al.*)	Liquid-Solid
D	Euler-Euler granular, standard k-ε model	Lu and Gidaspow (Modified model)	Gunn Model (Heat Transfer)	Gas-Solid
E	Euler-Euler dispersed, standard k-ε model	Syamlal-O'Brien	Adsorption model DME-SR models (Reaction)	Gas-Solid
F	Euler-Euler dispersed, Euler-Lagrange, standard k-ε model	Wang	-	Gas-Liquid-Solid

Table VIII.   Information on how the mentioned CFD simulations were approached

Case	Objective	Validation	Problems
A	Study on mass transfer models	$k_L a$ in typical industrial bioreactors; Experimental data	Limited experimental data Fixed bubble size (expected coalescence) Bad mixing rate due to geometry
B	Study the influence of geometry on the reactor hydrodynamics and investigate various operating conditions	-	-

Table VIII. (Continues…)

Case	Objective	Validation	Problems
C	Study mixing phenomenon and spreading of the solid particles; Study impacts of secondary flows on particles; Development of a validation tool	Literature reviews on similar processes CFD results	No experimental data available; Complex geometry; Lack of turbulence modulation; Coupling of the dispersed and continuous phases
D	Improve the performance of the FCC regenerator with a new design of introducing solids into the system	Comparison with theoretical and industrial values with 2D validation	Lack of proper validation for UDF
E	Developing model for the steam reformation of DME to predict hydrogen production	Simulating an experimental work and comparison with the data; Literature reviews	Limited commercial validation; Limited information regarding the kinetics of other catalysts; Euler-Lagrange model not used due to increased simulation time
F	Comparing mixing of two industrial scale gas-liquid reactors	Comparison with impeller manufacturer data, experimental data and between the two reactors	Standard k-ε model underpredicting turbulence

It should be noted that in Table VII only one of the simulations is performed with realizable k-ε and the rest are using the standard model. The problem with standard k-ε model is that in highly turbulent systems, it might give non-physical values for the normal stresses and that is "non-realizable". (Shih *et al.* 1995) The realizable k-ε model will be introduced more in Governing Equations chapter (Chapter 5).

4 GEOMETRY AND MESHING IN CFD

In order to simulate a process in CFD, a 2D or 3D-model (geometry) and a computational domain that is split into smaller elements (mesh grid) are required. The model defines the structure of computational domain and is advised to be quite simple since this will affect the generation of mesh. The grid designates elements on which flow is solved and has cells that are grouped into boundary zones, which have boundary conditions (See Chapter 6). This chapter will provide information on how geometry and mesh should be treated in order to ensure more stable simulations.

4.1 Geometry of Reactor in CFD

When creating a model for a reactor, it is important to keep geometry itself quite simple. There is no need to go into details with every possible small object inside the reactor itself if these have hardly any influence on the flow field characteristics. Created geometry will also affect mesh, which will be discussed in the next section, as it makes generation of mesh harder to be kept structured. Thus unnecessary objects will only increase the mesh count, simulation time and the mesh becomes time-consuming to create. This can be caused by complex shapes such as bent blades of impeller or some insignificant equipment inside tank that do not affect overall flow. (Versteeg and Malalasekera 2007; Khare *et al.* 2009) An example of simplifying geometry for CFD modeling purposes is shown in Figure 10, where initial tank has a sensor in it, but since it does not affect overall behavior of system, it is removed.
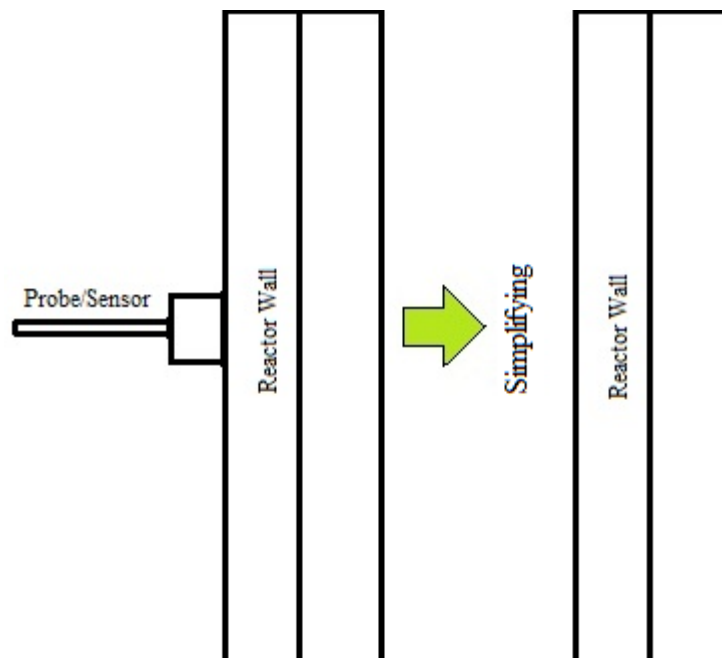

Figure 10.   Geometry simplification before meshing.

4.2 Meshing

Meshing is important in terms of splitting the computational domain into small control volumes. These control volumes are then used by software to calculate fluid parameters such as pressure, temperature and velocity. Quality of mesh should be kept high and cells

aspect ratios should be as regular as possible in order to resolve fluid flow accurately. (Blazek 2005) In terms of meshing a stirring reactor or in this case draft tube reactor, it is crucial to improve mesh quality and size to finer nearby areas where variables gradients are high, such as vortices and volume around a spinning impeller. Control volumes (cells) in spinning area affect the rest of system most in terms of introducing fluid velocity and in this case distribution and dispersion of gas. The rest of system should also be meshed so that control volumes are uniform in order to reduce error that is caused with the growth in volume size. Therefore, it is important to set a minimum and maximum cell size before creating mesh. It is advised that mesh size growth rate between adjacent elements should not exceed 1.25. Otherwise error in calculations will grow as CFD-software cannot properly predict how the gradients behave in adjacent cells. (Andersson *et al.* 2012) Refining of mesh is presented in Figure 11. In general, the importance of mesh quality depends on application (e.g. Often in multiphase simulations it is more important than in single phase).
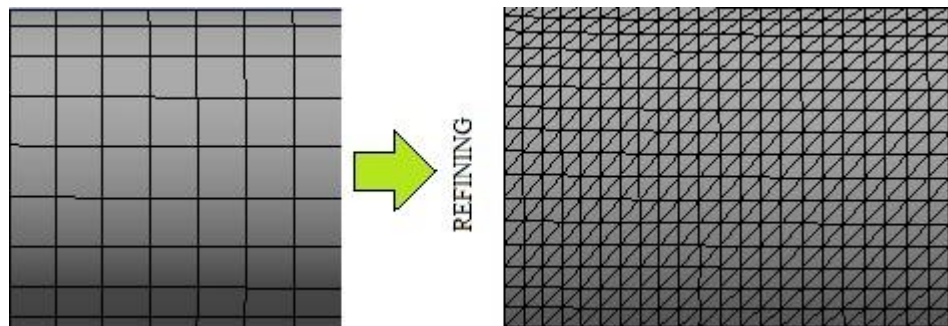

Figure 11.   Increasing the cells in mesh.

There is also issue with skewness of nodes as geometry of mixing tanks are hardly ever shaped as rectangular due to poor mixing efficiency, but rather cylindrical or ovoid. This will cause slight error depending on how skew element is. Also, additional geometry that was presented in Geometry section will introduce skewness to mesh as can be seen from Figure 12, where the mesh transforms from uniform mesh into unstructured mesh (Note that this mesh was created by 2D means, so in 3D it would introduce higher degree of skewness!). The impact of additional geometry to skewness can be reduced by refining mesh around objects to be more uniform. This however, takes extra time from user and if object has hardly any impact on process, then it is just better to remove it.
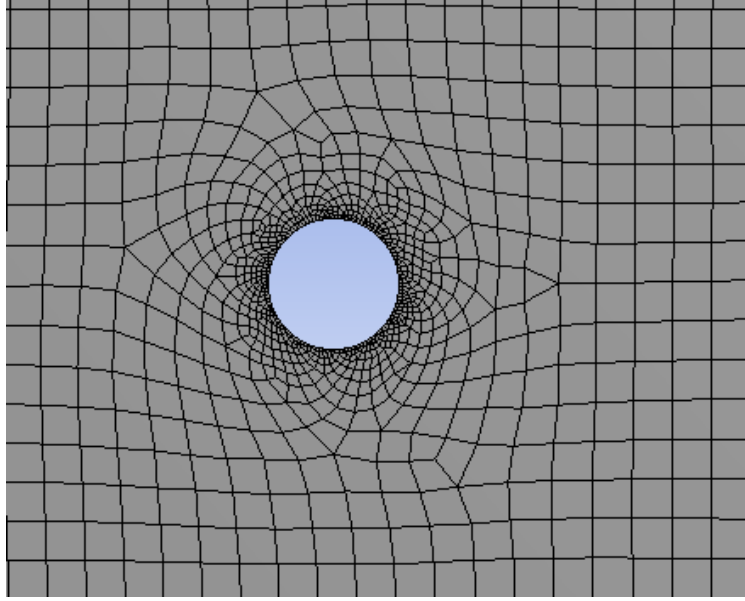
Figure 12.   The effect of additional geometry on meshing.

In a scenario where a study is made on a new system, it is recommended to perform a mesh independency test. Meshes of different cell numbers are used in a test-case simulation and results are compared to each other based on set objective for **(1)** time it takes to simulate and **(2)** how accurate results must be. For instance, the earlier mentioned study on dual fluidized bed reactor (Case E) had a mesh independency test made with grids of 117k cells up to 1.8M cells. Since the result differences between 117k - 400k cells were insignificant for the selected process variables and 1.8M cells took too much computational time, 117k was chosen to be used in the simulations.

5   GOVERNING EQUATIONS

Meshing is important in terms of splitting the computational domain into smaller control volumes. The governing conservation equations are iteratively solved in each and every control volume by a CFD-software and are constantly changing depending on initial values. This is why it is important for mesh to be uniform in order to ensure good accuracy for results. The theory behind mathematical means of governing equations will take place in this chapter.

5.1 Multiphase Modeling

This thesis will study hydrodynamics of gas-liquid system, where liquid will be the continuous phase and gas will be the dispersed phase. For this kind of system either volume of fluid (VOF), Euler-Euler or Euler-Lagrange model is normally used. The VOF model is typically used for surface tracking. Euler-Euler model is specifically good for processes where the motion of fluid is wanted to be observed on specific locations through space and time. Euler-Lagrange model, however, is more interested in the movement of particle inside fluid motion as it moves through space and time and how it interacts with other particles. (Marshall and Bakker 2004) If there are more particles to track in the system than computational cells (e.g. higher gas feeds in industrial scale), Lagrangian specification takes more computational effort (Zhang and Chen 2007). Thus only Eulerian specification for gas-liquid systems will be discussed about in this section.

The Euler-Euler multiphase model is designed for systems that contain two or more interpenetrating fluids. These can either be gases, liquids or solids. The volume fraction for any phase is not limited, so even small feeds can be observed with proper physical equations and analyzing methods. Each of fluids simulated will possess their own set of continuity and momentum equations. The interaction between phases will be incorporated through exchange terms in equations (e.g. momentum, heat, continuity) and phases are assumed to share cell domains proportionally, making the sum of the volume fractions (α) for liquid (*L*) and gas (*G*) in a cell domain:

$$\alpha_L + \alpha_G = 1.0 \qquad (1)$$

The beauty of multiphase modeling is that all fluids that are treated in the system do not have to be bound by same physical equations. For example, these can be modified to be phase specific with different models for drag, lift forces or turbulence or even correlations for the existing ones to reflect process better. However, there must be an exchange term between equations of separate phases. Otherwise, the interaction between them cannot be coupled. (Marshall and Bakker 2002)

5.2 Conservation of Mass

Conservation of mass or the continuity equation is basically the starting point for simulations to take place. All fluid properties are functions of space and time so it can be expressed by property(x,y,z,t). This is visualized in a block form shown in Figure 13.
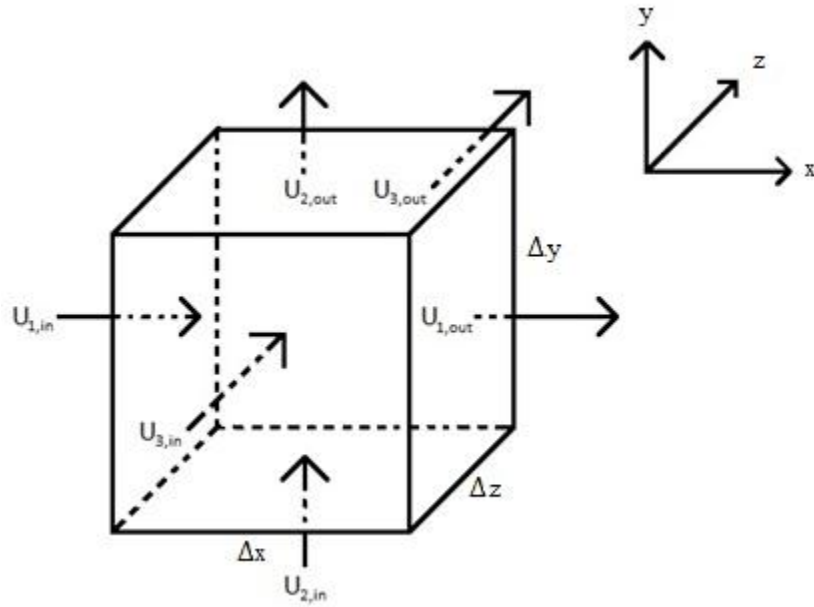

Figure 13.   A rectangular control volume to represent fluid inflows and outflows.

Spatial dimensions of a block can be expressed by its ribs lengths Δx, Δy and Δz and velocity components as U_1, U_2 and U_3 for each coordinate direction. In order to conserve the mass inside the control volume, the sum of inflow and outflow components through all six faces must equal zero. If we consider the property as density in incompressible systems, it can be expressed as

$$\rho\left(U_{1,out} - U_{1,in}\right)(\Delta y\Delta z) + \rho\left(U_{2,out} - U_{2,in}\right)(\Delta x\Delta z) + \rho\left(U_{3,out} - U_{3,in}\right)(\Delta x\Delta y) = 0 \qquad (2)$$

When the equation is divided by $(\Delta x\,\Delta y\,\Delta z)$, it takes a form of:

$$\rho\frac{\Delta U_1}{\Delta x} + \rho\frac{\Delta U_2}{\Delta y} + \rho\frac{\Delta U_3}{\Delta z} = 0 \qquad (3)$$

This may also be presented in differential form:

$$\rho \frac{\partial U_1}{\partial x} + \rho \frac{\partial U_2}{\partial y} + \rho \frac{\partial U_3}{\partial z} = 0 \tag{4}$$

Generally the density can vary in time and space, making the continuity equation take a form known as:

$$\frac{\partial \rho}{\partial t} + \frac{\partial}{\partial x_i}(\rho U_i) = 0, \tag{5}$$

where U_i is the ith component of fluid velocity and ∂x_i is partial derivate with respect to one of the three coordinate directions. (Marshall and Bakker 2002)

5.3 Momentum

The momentum equation is made on basis of Newton's second law, which states that the change of momentum is sum of forces in each of the three component directions that affect the fluid particle. It can be expressed as:

$$\frac{\partial(\rho_i U_i)}{\partial t} + \frac{\partial}{\partial x_j}(\rho_i U_i U_j) = -\frac{\partial p}{\partial x_i} + \frac{\partial}{\partial x_j}\left[\mu\left(\frac{\partial U_i}{\partial x_j} + \frac{\partial U_j}{\partial x_i} - \frac{2}{3}\frac{\partial U_k}{\partial x_k}\delta_{ij}\right)\right] + \rho g_i + F_i, \tag{6}$$

where the convection terms are on the left and the terms on right are respectively the pressure gradient, divergence of the stress tensor, gravitational force and other generalized forces. The divergence of stress tensor on the right side is responsible for the diffusion of momentum. Momentum equation is part of collectively called the Navier-Stokes equations, which contain also transport by convection, diffusion and several momentum sources in addition to just momentum.

5.4 Turbulence

Regime of fluid flow is classified based on dimensionless Reynolds number, which is defined as the ratio of inertial to viscous forces. The general form for Reynolds number is:

$$Re = \frac{\rho UL}{\mu},$$

(7)

where L is the characteristic linear dimension and μ is the dynamic viscosity of the fluid. For mixing tanks Reynolds number is defined by:

$$Re = \frac{ND^2\rho}{\mu},$$

(8)

where N represents the rotational speed of the impeller and D is diameter of the impeller. Usually for mixing tanks Re of over 10,000 means that the mixing regime is fully turbulent and anything between 1,000 and 10,000 means that the mixing regime is transitional. Values below 1,000 can be treated as laminar. (Holland and Bragg 1995)

There are several methods for turbulence to be introduced into Navier-Stokes equation. Most of the models involve time-averaging the conservation equations. So as turbulence gets included, the transported quantity is assumed to be the sum of equilibrium and fluctuating component that in case of velocity, for instance, can be expressed as $U_i + u_i'$. After time-averaging over many cycles of fluctuation, terms containing the factors of fluctuating component average to zero. This can be expressed as:

$$\lim_{t \to \infty} \frac{\partial u_i'}{\partial t} = 0$$

(9)

The only term remaining positive definite is the one that contains the product of two fluctuating terms. The remaining terms are identical to those of momentum Eq. (6). This gives form to the so called Reynolds-Averaged Navier-Stokes (RANS) for momentum:

$$\frac{\partial(\rho U_i)}{\partial t} + \frac{\partial}{\partial x_j}\left(\rho U_i U_j\right) = -\frac{\partial p}{\partial x_i} + \frac{\partial}{\partial x_j}\left[\mu\left(\frac{\partial U_i}{\partial x_j} + \frac{\partial U_j}{\partial x_i} - \frac{2}{3}\frac{\partial U_k}{\partial x_k}\delta_{ij}\right)\right]$$
$$+ \frac{\partial}{\partial x_j}\left(-\rho\overline{u_\iota' u_J'}\right) + \rho g_i + F_i,$$

(10)

where the term on right hand side, $\overline{u_\iota' u_J'}$, is time-averaged value for Reynolds stresses. The accent on the term is to notify of time-averaged value. As Reynolds stresses are introduced as new unknowns to the equations, they need to be related to the other variables. Reynolds stresses are system specific, which is why variety of turbulence models has been created for the purpose of solving them. Most of these are related to the Boussinesq Hypothesis, which makes the assumption that the Reynolds stresses can be expressed in terms of mean velocity and its variation:

$$\rho_i\overline{u_\iota' u_J'} = \frac{2}{3}\rho_i k\delta_{ij} + \left[\mu_t\left(\frac{\partial U_i}{\partial x_j} + \frac{\partial U_j}{\partial x_i}\right)\right]$$

(11)

where new constant, μ_t, called turbulent viscosity or eddy viscosity is introduced. When the Boussinesq Hypothesis Eq. (11) is added to RANS equation Eq. (10), the terms that contain partial derivatives can be combined. Now the combined viscosity takes a form known as the effective viscosity:

$$\mu_{eff} = \mu + \mu_t$$

(12)

Turbulence kinetic energy is the second new term to be introduced, which is defined in terms of velocity fluctuations in the coordinate directions:

$$k = \frac{1}{2}\left(\overline{u'^2} + \overline{v'^2} + \overline{w'^2}\right)$$

(13)

These new unknown parameters in the Boussinesq Hypothesis Eq. (11) are computed through the use of turbulence model. As mentioned before, there are several methods for turbulence to be introduced into Navier-Stokes equations in CFD-software. These include 2-equation turbulence methods such as standard k-ε model, re-normalization group (RNG) k-ε model, realizable k-ε model, k-ω model and Reynolds stress (RSM) model. Most of the

models involve time-averaging the conservation equations. Besides the 2-equation models, there is detached eddy simulation (DES), direct numerical simulation (DNS), large eddy simulation (LES) and more. DNS solves all scales accurately, whereas LES is used to model small scales and big turbulence scales are accurately solved. DNS and LES however need fine grid resolutions and therefore are impractical for industrial cases due to massive amount of computational effort required for solving. DES is a mixture of RANS and LES model, where the model gets switched based on the resolution of the grid. (Andersson *et al.* 2012)

Since the system studied in this thesis contains high Reynolds number (=fully turbulent), has swirling flows and recirculation of fluid, a two-transport equation model that was proposed by Shih *et al.* (1995), the realizable *k-ε* model, is used. This is an improved version of the standard *k-ε* model. The problem with the standard *k-ε* model is that in highly turbulent systems it might give non-physical values for the Reynolds stresses, whereas realizable *k-ε* model has proven to provide improved predictions for the spreading rate of planar and round jets (Andersson *et al.* 2012). The realizable *k-ε* model can be expressed as:

$$\frac{\partial(\rho k)}{\partial t} + \frac{\partial}{\partial x_i}(\rho k U_i) = \frac{\partial}{\partial x_i}\left[\left(\mu + \frac{\mu_t}{\sigma_k}\right)\frac{\partial k}{\partial x_i}\right] + G_k + G_b - \rho\epsilon - Y_M + S_k \tag{14}$$

$$\frac{\partial(\rho\epsilon)}{\partial t} + \frac{\partial}{\partial x_i}(\rho\epsilon U_i) = \frac{\partial}{\partial x_i}\left[\left(\mu + \frac{\mu_t}{\sigma_\varepsilon}\right)\frac{\partial\epsilon}{\partial x_i}\right] + \rho C_1 S\epsilon - \rho C_2 \frac{\epsilon^2}{k + \sqrt{v\epsilon}} + C_{1\epsilon}\frac{\epsilon}{k}C_{3\epsilon}G_b$$
$$+ S_\epsilon \tag{15}$$

where

$$C_1 = max\left[0.43, \frac{\eta}{\eta + 5}\right], \ \ \eta = S\frac{k}{\epsilon}, \ \ S = \sqrt{2S_{ij}S_{ij}}.$$

In the transport equations G_k represents the generation of turbulence kinetic energy due to the mean velocity gradients. G_B also is generation of turbulence kinetic energy, which is due to buoyancy. Y_M represents the contribution of the fluctuating dilatation in compressible turbulence to the overall dissipation rate. C_2 and C_3 are empirical constants,

σ_k and σ_ϵ are the turbulent Prandtl numbers for k and ϵ and S_k and S_ϵ are user-defined source terms. Table IX presents the model constants and the new unknowns.

Table IX. Realizable k-ε model constants and effects on turbulence (Fluent manual 2016)

$$S_{ij} = \frac{1}{2}\left(\frac{\partial u_i}{\partial x_j} + \frac{\partial u_j}{\partial x_i}\right) ; \; C_{1\epsilon} = 1.44; \; C_2 = 1.9; \; \sigma_k = 1.0; \; \sigma_\varepsilon = 1.2$$

Turbulent viscosity:

$$\mu_t = \rho C_\mu \frac{k^2}{\varepsilon} \qquad \| \; C_\mu = 0.09$$

Turbulent Production:

$$G_k = -\rho \overline{u'_i u'_j} \frac{\partial u_j}{\partial x_j} \; G_k = \mu_t S^2$$

Effects of Buoyancy:

$$G_b = \beta g_i \frac{\mu_t}{Pr_t} \frac{\partial T}{\partial x_i} \; \beta = -\frac{1}{\rho}\left(\frac{\partial \rho}{\partial T}\right)_p \; Pr_t = 0.85 \; C_{3\epsilon} = tanh\left|\frac{v}{u}\right|$$

v, flow velocity parallel to the gravitational vector

u, flow velocity perpendicular to the gravitational vector

β, thermal expansion coefficient

Effects of Compressibility:

$$Y_M = 2\rho\epsilon M_t^2 \; M_t = \sqrt{\frac{k}{a^2}}$$

a, speed of sound

M_t, Mach number

5.5 Interfacial Momentum Exchange

Gas-liquid multiphase has interaction between the primary phase (liquid) and the secondary phase (gas). The most important interfacial interphase force in this kind of system is the force which acts on the bubbles that is a result from the mean relative velocity between the phases, the turbulent drag force. Other forces such as lift force and added mass force may also be significant under the velocity gradient of the surrounding liquid and acceleration of bubbles respectively. However a study made by Scargiali *et al.* (2007) confirmed that the application of interest in this work, gas-liquid stirred vessels, are essentially dominated by drag, buoyancy and convection. The system under study also had

relatively low gas volume per vessel volume per minute (*vvm*) so only the drag force had the most significant impact on the flow and the influence of the lift force on air bubbles inside the tank is negligible. This was also suggested by previous studies made by Lane *et al.* (2002) and Khopkar and Ranade (2006). That is why the rest of the forces are not discussed about in this section. Drag force that is proportional to the mean velocity difference, $\vec{R}_i$ is given by the following form:

$$\vec{R}_L = -\vec{R}_G = K_{GL}(\vec{U}_G - \vec{U}_L),$$ (16)

where K_{GL} is the gas-liquid exchange coefficient expressed as:

$$K_{GL} = \frac{3}{4}\rho_L \alpha_L \alpha_G \frac{C_D}{d_B}|\vec{U}_G - \vec{U}_L|$$ (17)

d_B is the bubble diameter and C_D is the drag coefficient defined as a function of the relative Reynolds number Re_p:

$$Re_p = \frac{\rho_L|\vec{U}_G - \vec{U}_L|d_B}{\mu_L}$$ (18)

For the calculation of the drag coefficient there are many different models, from which the standard correlation of Schiller-Naumann proposes that (Schiller and Naumann, 1935):

$$C_D = \begin{cases} \dfrac{24\left(1 + 0.15Re_p^{0.687}\right)}{Re_p} & Re_p \leq 1000.0 \\ 0.44 & Re_p > 1000.0 \end{cases}$$ (19)

Schiller-Naumann assumed that the particle size and shape is a relatively small non-deformable sphere. However, it is a basic drag model that does not necessarily apply to particles moving in a turbulent liquid as it was designed for rigid particles in laminar flow. That is why a modification to the correlation was introduced by Lane *et al.* (2006). It was based on a curve fit of available stirred tank drag coefficient data found from literature.

Lane noticed that there is a relationship between the ratio of the slip velocity (U_{slip}) to the particle terminal velocity (U_T) and therefore drag coefficient gets the following form:

$$\frac{C_D}{C_{D0}} = \left(\frac{U_{slip}}{U_T}\right)^{-2}, \tag{20}$$

where the ratio of U_{slip}/U_T is dependent on the Stokes number:

$$\frac{U_{slip}}{U_T} = 1 - 1.4Stk^{0.7}e^{-0.6Stk}, \tag{21}$$

which can be defined by:

$$Stk = \frac{\tau_B}{T_L} \tag{22}$$

τ_B is the particle (bubble) relaxation time and T_L is the integral time scale. The relaxation time for the bubbles (τ_B) can be presented as:

$$\tau_B = \frac{U_T}{2g} \tag{23}$$

T_L represents the characteristics of a turbulent flow which can be calculated as:

$$T_L = 0.135\frac{k}{\varepsilon} \tag{24}$$

5.6 Mass Transfer

Mass transfer in stirred vessels is reported in terms of k_La values. In simulations the mass transfer coefficient is determined by different models. These can either be used to predict mass transfer in advance or used to design a system based on the desired outcome, reducing the amount of trial and error work. Based on study made in Case A and summarized by Kulkarni (2007), the penetration model that is based on Higbie's

penetration theory of interface transfer is used to calculate mass transfer coefficient in this study:

$$k_{L\ penetration} = \frac{2}{\sqrt{\pi}} \sqrt{D_L \frac{\varepsilon}{\nu}},$$ (25)

where D_L is the gas diffusivity in liquid and ν is the kinematic viscosity. The model assumes that the mass transfer occurs mainly due to the effect of small eddies. (Higbie 1935) It is dependent on the turbulence dissipation rate, which can be obtained from the k-ε model.

Bubble size plays a significant role in mass transfer as the interfacial area between phases is dependent on gas fraction and the diameter of bubbles. In case of a constant bubble size, the interfacial area between phases can be calculated with

$$a = \frac{6\alpha_G}{d_B}.$$ (26)

In the end, user selects models for describing multiphase effects, turbulence, drag model etc. Thus the user's choices will have an impact on the accuracy of the results. In industry the goal of CFD modeling projects might differ from that in academy. In academy, it is important to accurately model what has been measured. In industry, it is enough to model well enough, then, accept that the actual situation might be somewhat different from modeling results. The main focus is to keep everything fixed in the modeling approach throughout the modeling project and still be able to predict the large scale effects and trends correctly. CFD in industry is a tool to help in design and trouble-shooting questions and one has to accept small inaccuracies in the results.

6 BOUNDARY CONDITIONS

Boundary conditions (B.C.) define the input and output values, based on which model will calculate the flow properties elsewhere in the computational domain. These include general applications like wall, pressure inlet, pressure outlet, velocity inlet and degassing outlet.

Each of these applications is also malleable by changing settings for one in CFD software or creating UDF. For instance, the velocity profile of introduced gas can be changed from being normal to boundary (x,y,z) to cylindrical in case there is experimental data on how the distribution should behave. This is good in terms of trying to make the simulation behave exactly like the experiment. If this is succeeded in, then problematic areas can be studied and improved by modifying the problematic areas in the simulation. In this study there is an impeller, gas inlet, gas outlet and the walls of the geometry that need to be defined. The general principles of different boundaries and their boundary conditions are explained in this chapter.

6.1   Impeller

In reactor studies such as this work, where there are rotating impellers, the rotation must be described by a CFD model. This section will briefly describe what kind of models there are available and what kind of limitations are related to them. There is also a section, which will explain how flooding of impeller affects mixing.

6.1.1 Multiple reference frame (MRF) Model

The multiple reference frame model is a modification of rotating frame model (Luo *et al.* 1994). Rotating frame model's idea was to solve the momentum equations by rotating the entire computational domain, however, this approach is only suitable for unbaffled tanks. MRF model used this idea, but instead of rotating the entire domain, only one or more rotating (or non-rotating) domains can be used in a simulation as can be seen in Figure 14. Both of these models include the Coriolis force in the process. Angular velocity of the primary rotating component is the angular velocity of the frame. However, since the impeller is static, the rotating frame rotates the opposite direction of intended**.** The difference to rotating frame model is that MRF model allows complex interiors to be stationary.
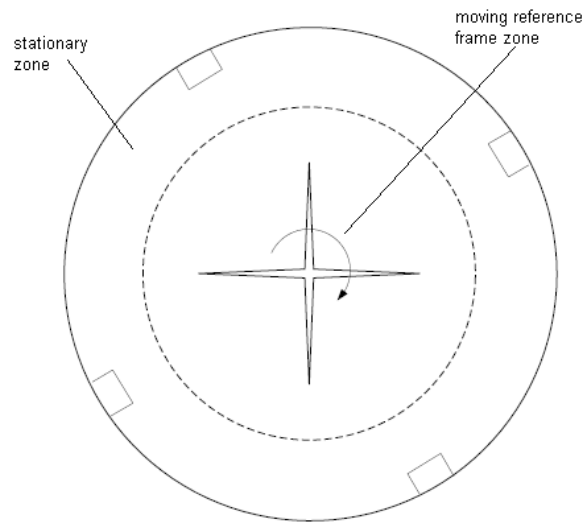
Figure 14.   The principle of MRF model. (Fluent manual 2016)

The pro of MRF method is that since it can be applied to multiple different impellers, they can have separate rotating frames with separate rotation frequencies, while the rest of the space can be modeled with a stationary frame. The con is that if there is a strong relation between the impeller and baffles, the solution with impeller in position relative to the baffles will be different from that with impeller in a different position as the impeller geometry itself is static, not moving. (Marshall and Bakker 2002)

6.1.2 Sliding Mesh (SM) Model

Sliding mesh model is the most informative and exact solution method for a stirred tank simulation. It is a time-dependent solution approach meaning that it is not suitable for steady-state simulations. The grid surrounding the rotating component(s) physically moves during solution. This model can capture even low frequency oscillations in the flow field (Bakker et. al. 2000; Roussinova *et al.* 2000) in addition to those that result from the periodic impeller-baffle interaction. In order to reach steady state, it will take dozens of revolutions and is time consuming as it requires plenty of simulation time. Sliding mesh model is presented in Figure 15.
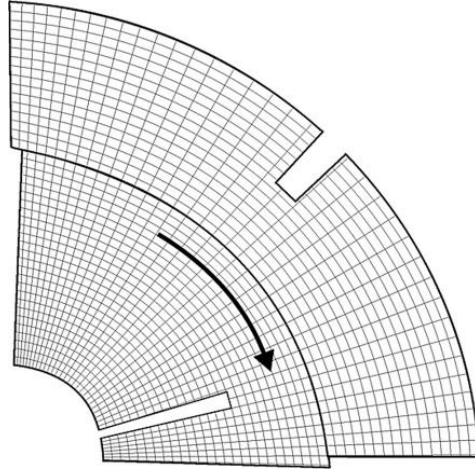
Figure 15.   The principle of SM model. (Andersson *et al*. 2012)

6.1.3 Impeller Boundary Condition (IBC) Model

The impeller boundary condition (IBC) model is one of the simplest ways to introduce impeller without having an actual geometry for the impeller. This model has a cylinder placed in the location of the impeller that represents the rotating zone (spinning volume) that the impeller creates. It uses the faces of the cylinder as velocity inlets with only the side imposing the spinning motion for the fluid. This is introduced by having a mass flow into the system on basis of velocity components (angular, axial, radial and tangential), which will generate the jet that impeller would make. In order to use this model, there needs to be some reference data from experiments to capture the ith velocity components with (e.g. PIV-measurement). (Brucato *et al.* 1998; Deen *et al.* 2002) As long as the geometrical ratio between the scaled-up version of the impeller zone and the laboratory size are similar, the velocity components should correlate with each other by the means of:

$$U_{i,fullscale} = \frac{U_{i,labscale}}{v_{tip,labscale}} \cdot v_{tip,fullscale} \tag{27}$$

When the power input and tip speed for the industrial scale are known, these can be used in order to determine the rotational speed of the impeller *N*:

$$N = \frac{v_{tip}}{\pi D} \tag{28}$$

When the rotational speed is known, the power number for the impeller N_P can be calculated with the following equation:

$$N_P = \frac{P}{\rho_L N^3 D^5} \tag{29}$$

6.1.4 Flooding of Impeller

The flooding point for a radial-flow impeller can be characterized through the means of using main dimensionless numbers: gas flow number Fl_G and impeller Froude number Fr, and the geometry. (Smith *et al.* 1987) Flooding means that below a certain minimum speed, the impeller no longer has discernible action, which can be expressed as:

$$Fr < 0.04 \tag{30}$$

Based on studies made by Nienow *et al.* (1985) on traditional stirred tank reactors, the flooding will occur as the gas flow will swamp the impeller and this will take place as:

$$Fl_G > 30 Fr \left(\frac{D}{T}\right)^{3.5}, \tag{31}$$

where

$$Fl_G = \frac{Q}{ND^3}, \quad Fr = \frac{N^2 D}{g}$$

Flooding is unwanted phenomenon as it will significantly reduce the dispersion of the gas in the system and through it the mass transfer rate between the phases will become worse. This is why it is important to identify the ratio between gas flow rate and impeller power input that can be used in order to obtain the most optimal conditions for the mass transfer to take place. (Nienow *et al.* 1985)

6.2 Gas Inlet, Outlet and Walls

There are many ways to introduce mass flow to a system and set different surface types such as walls in CFD-software. However some of these come with limitations (e.g. software specific) that may affect the simulation stability. This section will describe what kind of inlets, outlets and walls are used in this work. These are also presented in Figure 16.
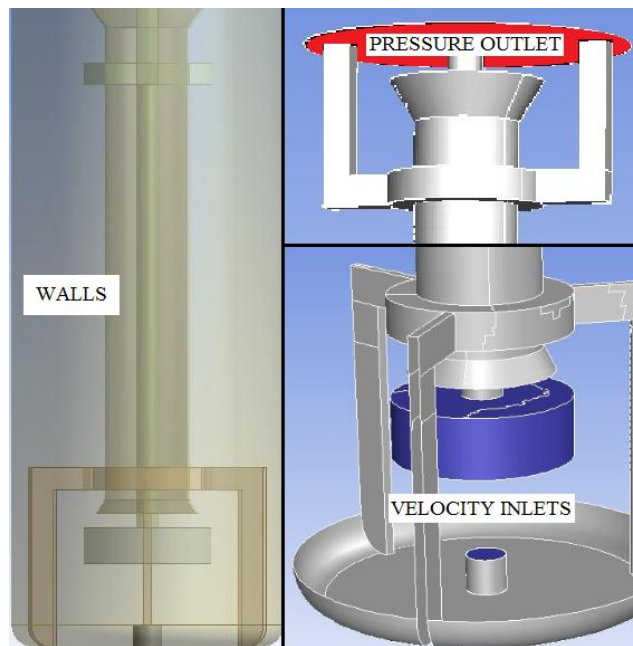

Figure 16. Simulation boundary conditions in this work

Inside the reactor regarding this work, there is a gas feed coming from the bottom of the reactor. This is introduced to the simulation as a velocity inlet. The top surface of the tank volume is treated as a pressure outlet. This could also be set as a degassing boundary condition in case MRF model was used for the impeller. The degassing boundary acts as a no-slip wall for primary phase (liquid) and allows the secondary phase (gas) to escape out of the system. However, since the IBC model (velocity inlet) for impeller introduces new continuous phase mass into the system, it will not be able to get out and this will cause a problem as the mass balance fails. The pressure outlet instead extrapolates the pressure from interior flow and requires a specification for static pressure at the boundary and a backflow ratio for the primary phase. The backflow or the reverse flow direction should be realistic in order to minimize convergence difficulties during simulation. (Fluent manual 2016)

The solid structures inside the reactor are set as no-slip walls that are treated with standard wall functions. These are based on the proposal of Launder and Spalding (1974) that affect the momentum for mean velocity yields by:

$$U^* = \frac{1}{\kappa}\ln(Ey^*), \tag{32}$$

where

$$U^* \equiv \frac{U_P C_\mu^{1/4} k_P^{1/2}}{\left(\frac{\tau_w}{\rho}\right)}, \qquad y^* \equiv \frac{\rho C_\mu^{1/4} k_P^{1/2} y_P}{\mu}$$

κ is von Kármán constant of 0.4817, E is an empirical constant of 9.793, U_P is mean velocity of the fluid at point P, τ_w is viscous shear stress near wall, k_P is the turbulence kinetic energy at point P, y_P is the distance from point P to the wall and C_μ is a turbulence model coefficient. The logarithmic law for mean velocity is applied in Fluent when $y^* > 11.225$ and below that laminar stress-strain relationship is used, which can be expressed as

$$U^* = y^* \tag{33}$$

These laws-of-the-wall for mean velocity in Fluent are based on the wall unit y^* rather than y^+, however the quantities are approximately equal in equilibrium turbulent boundary layers. The principle of wall functions is to capture the change in fluid velocity profile near the wall as can be seen in Figure 17. The general recommendation for a standard wall function at high Re is the range of $30 > y+ > 500$ and the first cell height y_c near the wall has to be refined accordingly:

$$y^+ \approx \frac{u_* y_c}{\nu}, \tag{34}$$

where u_* is the characteristic velocity scale for the sub-layers given by $u_* = \sqrt{\tau_w/\rho}$.
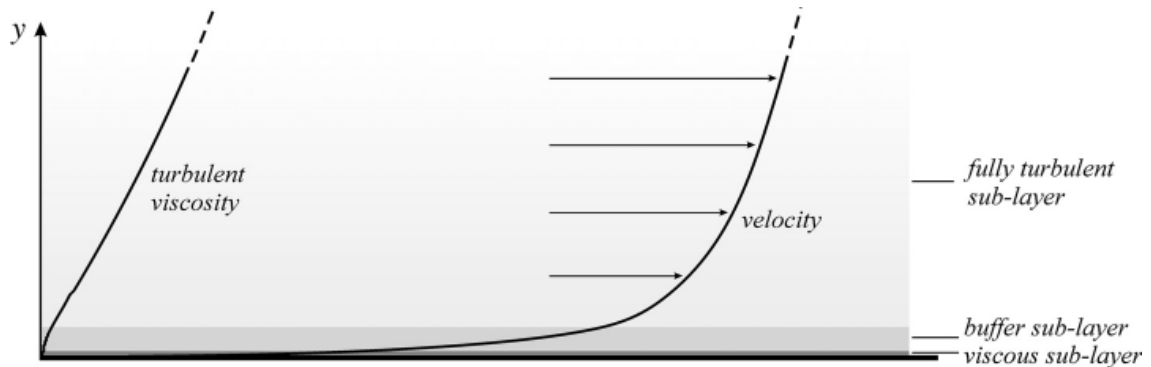
Figure 17. Velocity profile near the wall due to sub-layers. (Andersson *et al.* 2012)

EXPERIMENTAL PART

Draft tubes are commonly in use for airlift reactor to enhance liquid circulation inside a tank axially. The tube is usually installed centrally within a vessel. Airlift reactors are pneumatically agitated reactors where flow is driven by buoyancy with an upflow channel (i.e., riser) and a downflow (i.e., downcomer) channel. Initial velocity is usually introduced from a sparger at bottom of riser by gas. Gas phase moves liquid phase upwards in riser until it disengages from liquid phase at the top of column. Liquid phase continues its flow down in downcomer taking some of gas phase that could not disengage from flow with it. This is caused by downwards velocity of liquid being greater than velocity of bubbles towards surface. Usually gas hold-up in downcomer however is much lower than in riser. (Chisti and Moo-Young 1988; Luo and Al-Dahhan 2007)

Draft tube's principle was to enhance circulation axially whereas in stirring reactor tank the idea is to distribute dispersion radially (unless impeller is made to have more horizontal distribution) and break bubbles into smaller diameters in order for gas phase to have as big surface area in fluid as possible to enhance mass transfer rates between phases. The general idea of both is demonstrated in Figure 18. Draft tube reactor that is used in this study is a combination of these two. So when pros of these two reactors are put together, mixing will ensure gas-dispersion inside the reactor radially and draft tube ensures better liquid circulation inside the reactor axially.
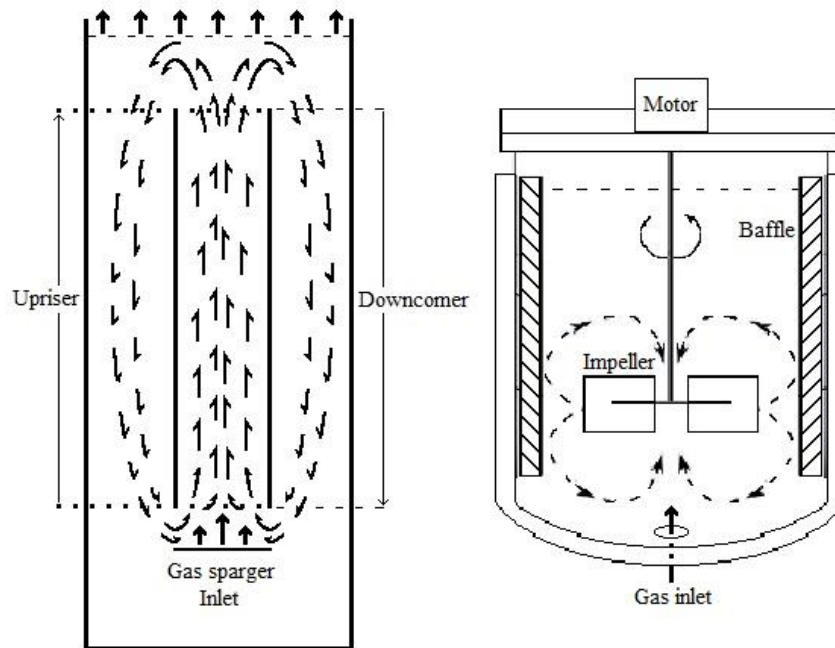
58

Figure 18. Liquid flow pattern in centrally fed airlift reactor (left) and stirred reactor tank (right).

According to study made by Tervasmäki *et al.* (2016) draft tube reactor has higher mass transfer rate compared to 3-impeller Rushton turbine mixing reactor with similar agitation power. Also, uniformity of dissolved gas was better in the agitated draft tube geometry. The sketches of the reactors studied can be seen in Figure 19.
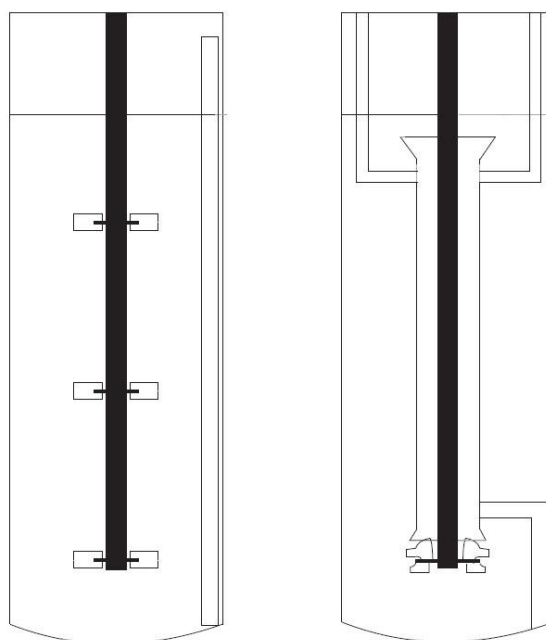

Figure 19. Reactors under study, Rushton (left) and OKTOP®9000 (right). (Tervasmäki *et al.* 2016)

7 SOFTWARE AND SIMULATIONS

The objective of this study was to simulate gas-liquid mixing in industrial scale draft tube reactor with a CFD-software. For the CFD simulations, the latest version (18.0) of ANSYS Fluent was used. The operating system was a 64-bit version Windows 7 and the hardware consisted of Intel i3-6100 @ 3.70GHz quad-core processor and 8GB RAM memory. All four cores were utilized during the simulations and double precision was set. Double precision is used as it is more accurate than single precision especially in systems where tiny relative differences are significant or meshes have a large difference between the largest and the smallest element sizes such as this study. Double precision also helps with solution stability. However, since double precision requires more memory, it can be concluded that 8GB of RAM memory was the bottleneck in simulation times.

7.1 Geometry

The main dimensions (height and width) were given as initial data for the simulation of industrial scale reactor. These are presented in Figure 20 with a 3D-model of the geometry. The sketch shows the main structures for the reactor. There are three baffles located on the bottom of the reactor that also serve as holders for the draft tube and two lid holders on the top. The actual reactor also has supporting structures for the draft tube in the middle of the reactor as can be seen in Figure 1, however, these were not included in the simulations.

The geometry used for the simulations was based on a laboratory scale model that got scaled-up to industrial size by using ANSYS Fluent's mesh and geometry scaling tool. The scaling factors used for width (x, y) were ~39.47 and height (z) ~47.45. The initial dimensions are listed in Table X.

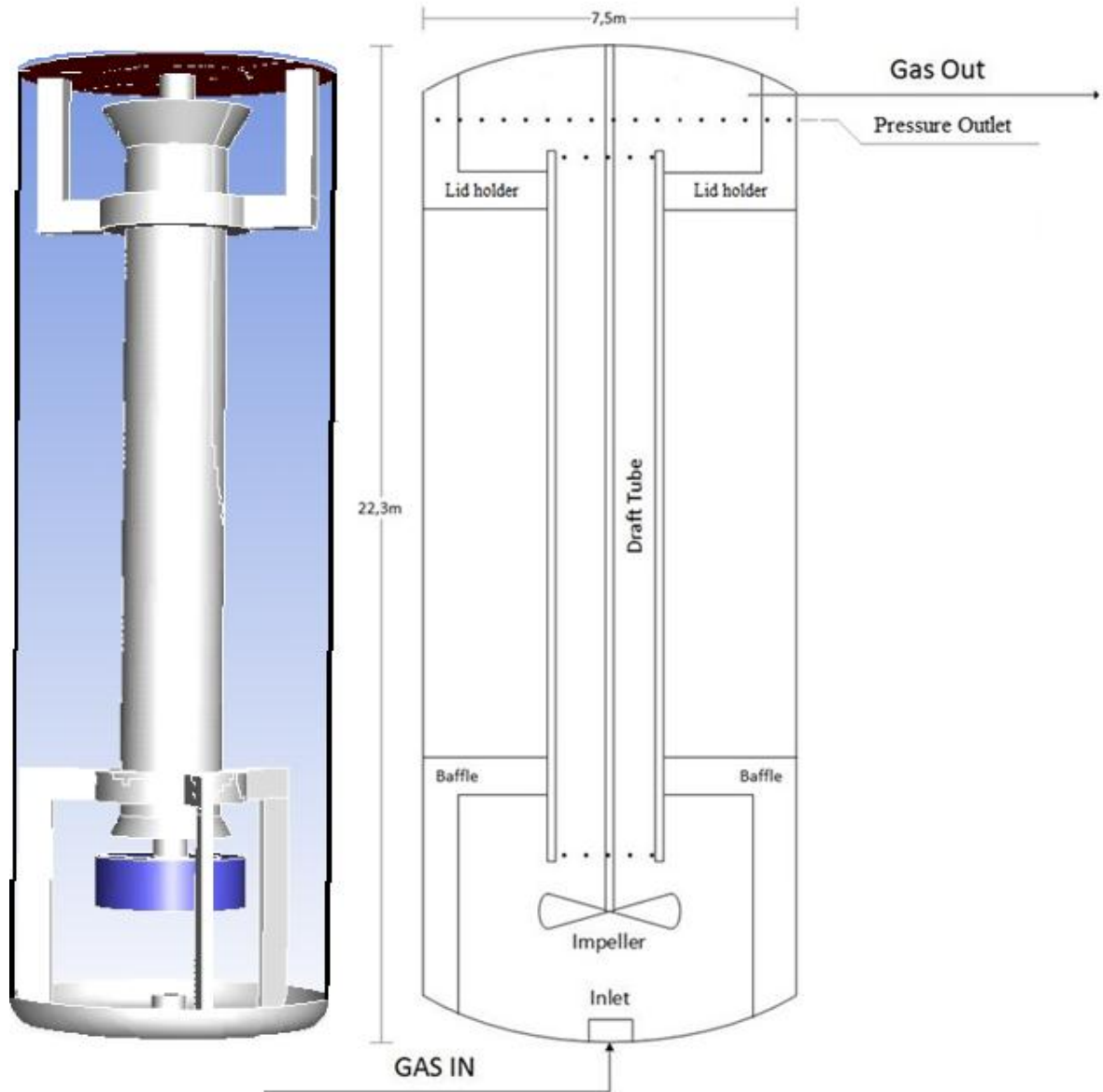**Figure 20.** OKTOP®9000 industrial scale reactor.

Table X. Laboratory and industrial scale draft tube reactor main dimensions

Scale	Laboratory	Industrial	Scaling Ratio
D_I (impeller)	79.0mm	3.12m	39.47
D_S (spinarea)	89.0mm	3.51m	39.47
C_I	25.0mm	1.19m	47.45
T	190mm	7.50m	39.47
H_T	470mm	22.3m	47.45
$D_S - D_I$	10.0mm	0.39m	39.47
V Total	13.3L	985m3	74000
V Fluid	12.6L	936m3	74000

7.2   Operating Conditions

Gas-liquid simulations were done using Euler-Euler SIMPLE pressure-based solver in steady-state. The considered 2 phases were a continuous phase of water-ethanol 3% solution (liquid) with surface tension of 0.06287N/m and a dispersed phase of air (gas). The microbes are of such a small size that they are treated as part of the continuous phase. The physical properties for the phases are taken from Fluent database (water and air at 25°C). These are listed in Table XI.

Table XI.   Physical properties of the phases in ANSYS Fluent

Phase	Material	Density (kg/m^3)	Viscosity (Pas)
Continuous	Water	998.2	$1 \cdot 10^{-3}$
Dispersed	Air	1.225	$1.789 \cdot 10^{-5}$

The gas feeds range from 1980 to 15000m^3/h at a constant impeller mixing intensity of ~0.28W/kg averaged over the whole fluid volume of 936m^3. Outlet is set as pressure outlet with static gauge of 0kPa. There was also a suggestion to try degassing (acts as a slip-wall for continuous phase) as the boundary condition for the outlet. However since IBC model is used for the impeller, the degassing will not let out the excess liquid introduced by the IBC model to the system and the mass balance fails.

7.2.1 Impeller and Gas Inlet

There was information from Outotec on the actual impeller main parameters, P = ~250kW, N_p = ~3.1 and v_{tip} = ~6.3m/s, which were taken into account when estimating the initial guess for impeller rotational speed. As the main purpose of the simulation was to get a rough understanding of how the gas-liquid system behaves, impeller boundary condition model was used for the simulations as it takes less computational effort than MRF model. IBC model required information on velocity profiles, which were acquired from laboratory scale model by PIV-measurement. These were then scaled-up for utility scale model based on Eq. 27. The problem with IBC model, however, is that it gives less accurate results as the impeller area (spinarea) is treated as a gray area, which is not included in the simulation. From Table X it can be noticed that the distance from actual impeller tip distance to the spinarea that is used with IBC method gets further with scale-up. Since the

height is scaled with different factor, the impeller's height to width ratio (C_I/D_S) was not kept constant and needed to be treated with UDF to limit the used area as presented in Figure 21, where the blue area has a discharge velocity set as 0m/s.
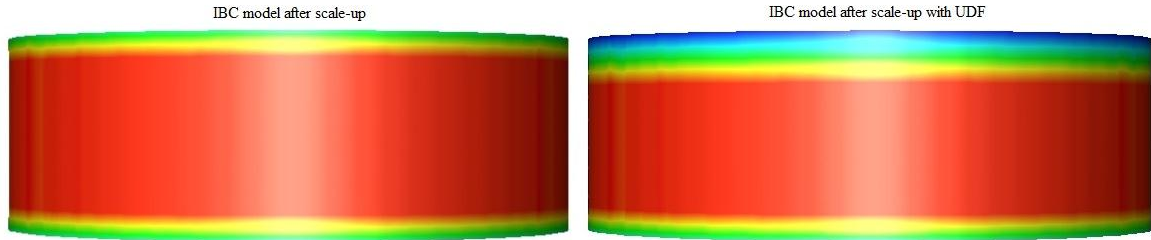

IBC model after scale-up   IBC model after scale-up with UDF

Figure 21.   Radial velocity contours at sweep of spinarea modeled without (left) and with (right) UDF keeping the geometrical ratio between height and width constant.

The distance difference between the spinarea and impeller diameter D_S - D_I was taken into account when imposing the rotational speed from the impeller based on the known values for the actual impeller. This was used as an initial guess to calculate ungassed power in the reactor based on the overall torque counted from the walls (T_Q):

$$P = 2\pi N T_Q \tag{35}$$

The overall torque from the walls was extracted from Fluent by taking force of moment related to z-axis using center of the spinarea as the origin point. Momentum was calculated by integrating torque values at reactor walls. The rotational speed for the IBC model in the simulations was determined from three different operational points in order to get power input of approximately 250kW accordingly to Figure 22.
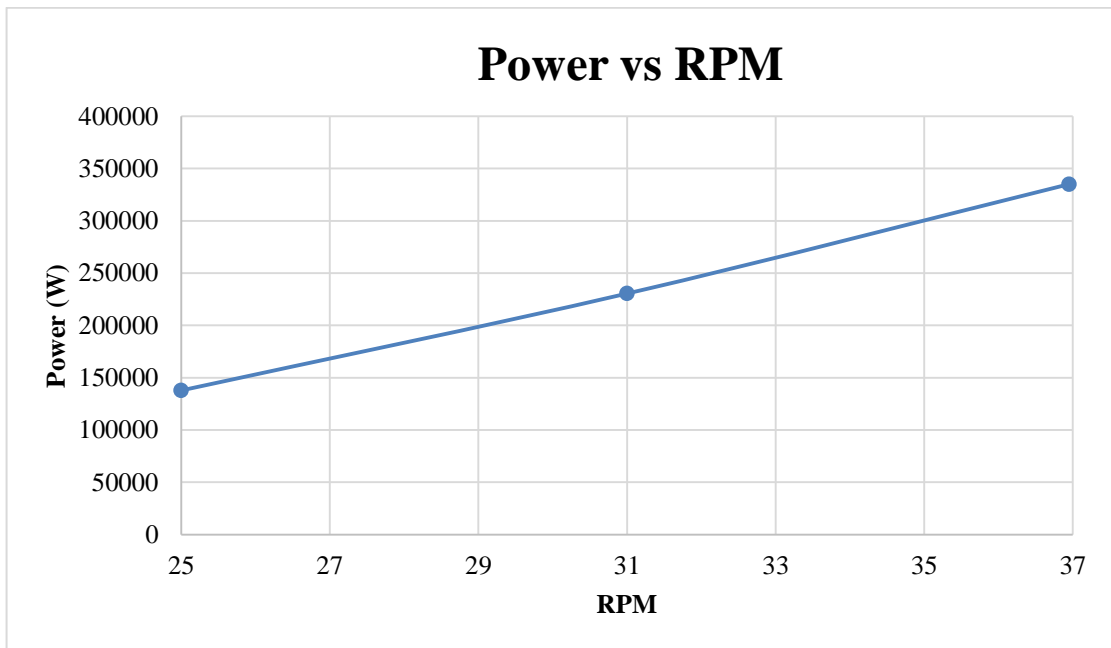
Figure 22.   Defining rotational speed for the impeller.

7.2.2 Bubble Size

Bubble size affects the hydrodynamics of gas as well as the interfacial area for the mass transfer to take place. Since average bubble size was decided to be used for the simulations to reduce computational effort and complexity, it had to be based on literature reviews on similar processes. Laakkonen *et al.* (2007) made a laboratory scale (200L) study on the behavior of bubble size in traditional stirred tank reactor based on mixing intensity (constant *vvm* of ~0.5) and *vvm* (constant mixing intensity of ~1.5W/kg). The surface tension of the study was for air-tap water, with measured surface tension of $\sigma = 0.069$N/m. The results from Laakkonen *et al.* are presented in Figure 23.
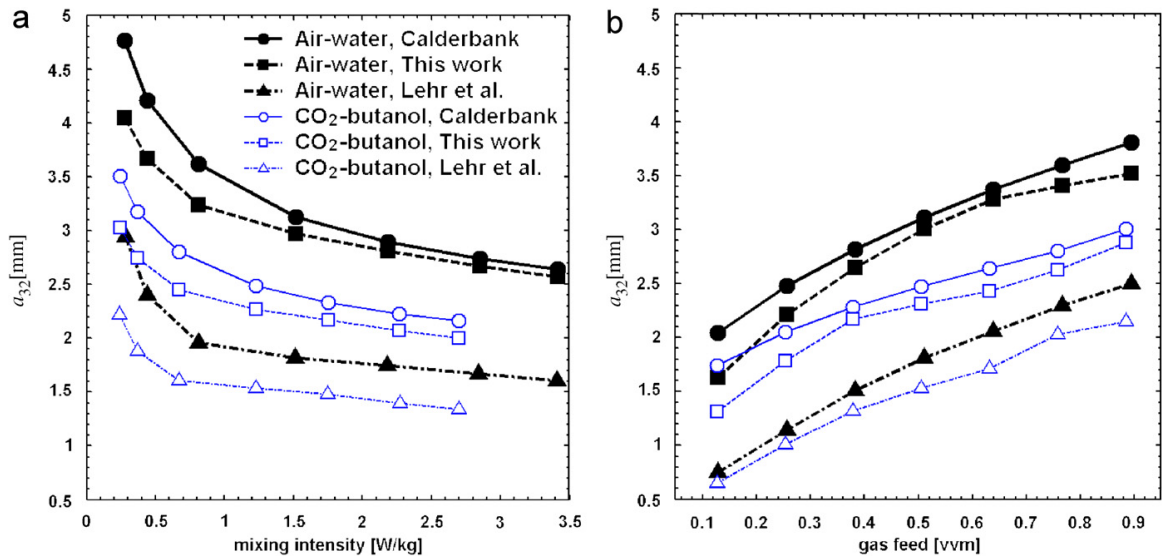
Figure 23. Vessel-averaged Sauter mean bubble diameter in agitated vessel with the effect of (a) different mixing intensity and (b) gas feed. (Laakkonen *et al.* 2007)

The simulations gas feed in this work range from 0.035 to 0.267*vvm* and the mixing intensity for the whole fluid volume is around 0.28W/kg. Average bubble size a_{32} (increase of 1.1mm) was determined based on Figure 23 (a) and (b) by matching reactor specific power input and *vvm* to fit actual simulation input data. Due to the gas feeds above normal operations ($\sim$4020m^3/h) the estimated average bubble diameter of 3mm was chosen to be used for the simulations. The basis for the chosen bubble diameter is presented in Figure 24. Bubble size was not defined as a function of reactor height, which could have been done with UDF.
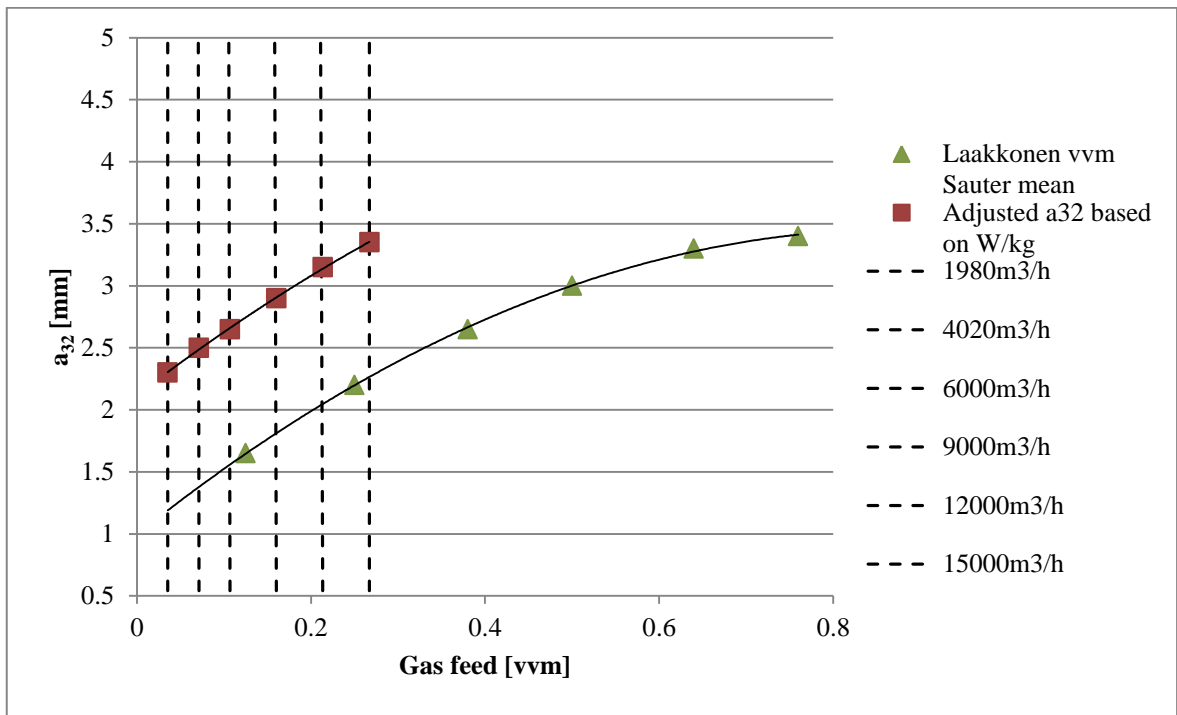
Figure 24.   Estimated average bubble size for the simulations.

There are a couple of factors that affect the bubble size: surface tension and mixing intensity in the bottom volume. The mixing intensity nearby the impeller area on the bottom of the reactor is around 1W/kg and the effect of ethanol decreases the surface tension of the system, which will also reduce coalescence of bubbles. (Machon *et al.* 1997; Besagni *et al.* 2016) Taking these into account the actual bubble size might actually be smaller from the average set in the simulations. However, since the reactor is industrial size, there might be more coalescence than experienced in laboratory experiments (Leng and Calabrese 2004). In the actual reactor, there is also the effect of hydrostatic pressure that is not included in the simulations, which would increase the solubility of dissolved gas in the bottom of the vessel and decrease bubble diameter (Tsao 2014).

7.3 Mesh Independence Test

When performing simulations for a new system, it is important to check how fine mesh is required for the simulation results to become grid independent. This is called mesh independence test where increasing the number of cells no longer affects the final results within a certain percentage. The laboratory scale model had been tested for mesh independency in previous FERMATRA study with 500k cells being fine enough, however

with the scale-up the volume of cells increased and new test was required to take place. The mesh created was structured hexahedral mesh. Figure 25 presents the overall mesh used in all of the simulations.
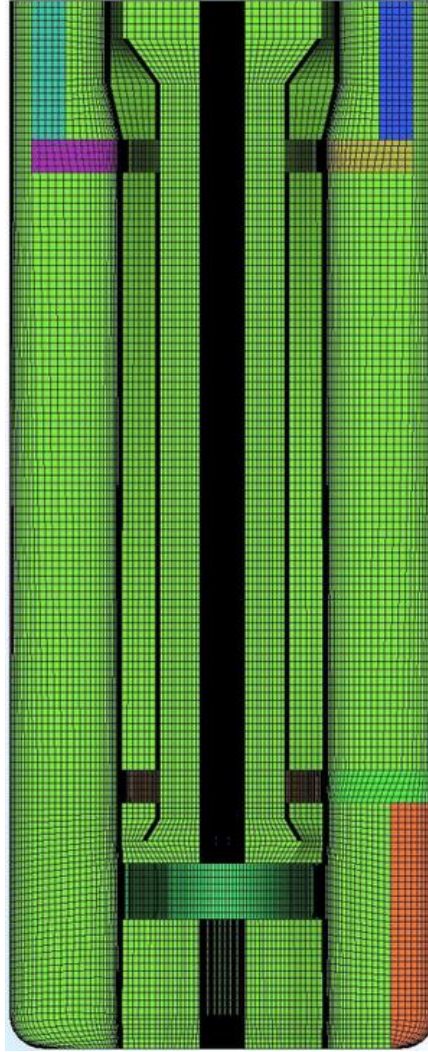

Figure 25.   Mesh used for CFD simulations

The mesh can be compared with each other by using normalized root mean square error (NRMSE) method (Wang and Zhai 2012):

$$NRMSE = \frac{3}{\left(\frac{cells_{Fine}}{cells_{Coarse}}\right)^{order} - 1} \sqrt{\frac{(variable_{Coarse} - variable_{Fine})^2}{variable_{Fine}{}^2}} * 100\% \qquad (36)$$

The results for the mesh independence test can be seen in Table XII.

Table XII.   Most important variables (volume integral values) that affect the system

Mesh	1	2	3	4
Cells	500k	1M	2M	3M
Simulation time (h)	8.8	15.8	25.7	40
k (m^2/s^2)	89.4	105.5	107.8	109.8
ε (m^2/s^3)	99.1	145.9	156.3	158.9
T_Q (Nm)	74260	86816	86957	88123
NRMSE (average)		61.8%	8.95%	9.56%

It can be seen that 500k is no longer accurate enough to be simulated with (NRMSE 43 to 96%), but between 1M, 2M and 3M cells the results for variables no longer vary as much (NRMSE 0.5 to 20%). According to the authors, grid difference can be considered negligible if NRMSE values are less than ~10%. This is why 1M cells mesh was used to run the simulations as it took the least computational effort. However, there were a couple of issues with the initial mesh, which had to be remade. First, the mesh on top of the draft tube was skewed and had to be remade in order to capture fluid movement on the top of the draft tube better. Second, there was an issue with $y+$ values being high near the walls ($\geq$ 2000) for continuous phase, that were above the range of $30 > y+ > 500$ and the first cell height had to be refined accordingly. With refined first cell height, the $y+$ values were reduced ($\leq$1000 in the most intense mixing area near the impeller) and the simulations were able to capture flow velocity near the walls better. After these modifications, the mesh size was roughly 1.7M cells and one simulation took roughly 18 hours. The modifications are presented in Figure 26.
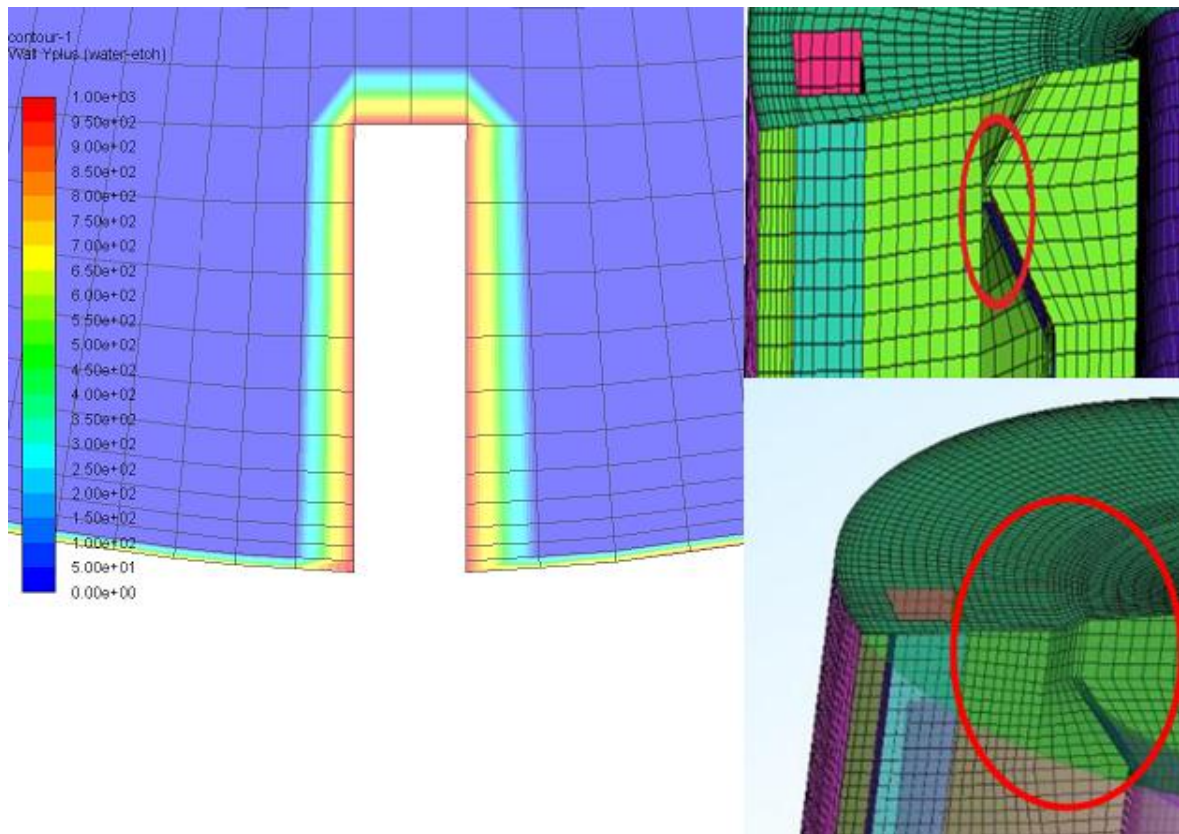
Figure 26. Refined first cell height to reduce continuous phase y^+ values nearby the most intense mixing zone in the bottom of the reactor (left) and refined mesh on top of the draft tube (right).

7.4 CFD Simulations (SETUP)

The simulations were done using SIMPLE pressure-based solver in steady-state with first order discretization for momentum and second order for turbulence. Transient simulation had also been tried on top of steady-state in order to see if there was any difference between the results. However, since both gave similar results to residuals and main variables, steady-state was used for less computational time. The bubbles were treated as non-coalescing due to the effect of ethanol and therefore bubble breakage and coalescence were neglected. The simulations matrix for the simulations is presented in Table XI.

Table XI.   Simulations matrix to evaluate the behavior of OKTOP®9000 reactor

		Simulations matrix:			
#	ungassed P/V (W/m^3)	Q (m^3/h)	d_B (mm)	Method	C_D
1	283	4020	3	Euler-Euler	**SN+Lane**
2	283	4020	3	Euler-Euler	**SN+Lane(Swarm)**
3	283	4020	**4**	Euler-Euler	SN+Lane(Swarm)
4	283	4020	**2**	Euler-Euler	SN+Lane(Swarm)
5	283	**1980**	3	Euler-Euler	SN+Lane(Swarm)
6	283	**6000**	3	Euler-Euler	SN+Lane(Swarm)
7	283	**9000**	3	Euler-Euler	SN+Lane(Swarm)
8	283	**12000**	3	Euler-Euler	SN+Lane(Swarm)
9	283	**15000**	3	Euler-Euler	SN+Lane(Swarm)

Turbulence was simulated with per-phase realizable k-ε model with an additional drag correlation that was defined by UDF. Schiller-Naumann (SN) model assumes that the particle size and shape is a relatively small non-deformable sphere. Based on the literature review on previous gas-liquid mixing in agitated reactors, there is a relationship between the ratio of slip velocity to the particle terminal velocity, which Lane's model counts for. However, since there might be some phenomena in industrial scale setup that are absent from laboratory and pilot scale setups, this study considered the impact of bubble swarm, where multiple bubbles affect each other increasing the gaseous phase velocity and drag coefficient as a function of gas hold-up. SN with Lane's correlation was compared to the proposed modified correlation, where Lane's correlation was introduced with the effect of bubble swarm by Roghair *et al.* (2013), which can be presented as:

$$\frac{C_D}{C_{D,\infty}} = \left[1 + \alpha_G \left(\frac{18}{E\ddot{o}}\right)\right](1 - \alpha_G), \tag{37}$$

where *Eö* is Eötvös number, which is a dimensionless number to characterize the shape of bubbles or drops moving in a surrounding fluid. The effect of swarm is valid for *Eö* ranging from 0.13 to 4.9, bubble diameters from 1 to 6mm and local gas fractions up to 40%. The results of the comparison are presented in Table XIII. The gas hold-up were volume averaged and mass transfer were calculated as volume integral over fluid volume.

Table XIII. Schiller-Naumann /w Lane's correlation vs. Schiller-Naumann /w Lane and effect of swarm presented by Roghair *et al.* (2013):

Name	P_G/V (W/m^3)	Q (m^3/h)	d_B (mm)	Gas hold-up (%)	k_La (1/s)
SN+Lane	282	4020	3	2.96	0.060
SN+Lane(Swarm)	243	4020	3	3.51	0.064

According to Table XIII Lane's drag model calculates gas velocity poorly due to bubble rise velocity since it only takes into account the effect of single bubble, whereas the added effect of swarm takes into account the impact of multiple bubbles affecting each other, which will increase the rise velocity of the bubbles. Lane's correlation with the effect of swarm is therefore used for further simulations.

8 RESULTS

The objective of this study was to simulate gas-liquid industrial scale draft tube reactor in order to see **(1)** how the distribution of gas inside the reactor and **(2)** k_La changes with different gas feeds while impeller power input is kept constant, **(3)** check when flooding point is achieved and **(4)** see how the change in average bubble size affects the gas hold-up and mass transfer results.

8.1 Data Points and Convergence

The simulations were carried with steady-state pressure-based simulation. The turbulence kinetic energy and dissipation rate could not be stabilized in order to get residual levels under 10^{-3} so the results were based on mass imbalance below 3%. The mass balance was monitored over outlet and inlet surfaces for both phases. However since this was a rough estimation on how the reactor behaves, higher values of 5% were also accepted. Typically the mass balance error (continuity) was $5 \cdot 10^{-4}$. Energy dissipation convergence error was around $1 \cdot 10^{-2}$ for liquid and gas phase. It was most likely caused by the relatively rough mesh (Deglon and Meyer 2006). There was an additional testing for error by simulating 500 iterations forwards in order to see how much variables (gas hold-up, torque and k_La) change. Based on the average error of 2% for each gas feed, error bars were introduced to the charts.

8.2 Bubble Sensitivity Analysis

There was also a bubble sensitivity analysis (3±1mm) for 4020 m^3/h gas feed where the main variables changed ~7% by average from the base case (#2). The results for different variables are presented in Table XIV. The gas hold-up were volume averaged values and the mass transfer values were calculated as volume integral over the fluid volume.

Table XIV.   Bubble sensitivity analysis simulations.

d_B mm	Mixing speed 1/min	Q m^3/h	Gas feed vvm	Gas hold-up %	k_La 1/s
4	33	4020	0.0716	3.21	0.061
3 (Base)	33	4020	0.0716	3.51	0.064
2	33	4020	0.0716	3.71	0.069

Bubble size sensitivity analysis shows physical behavior in the sense that with larger bubbles, the contact area between phases will reduce and this affects the mass transfer. Also the velocity of larger bubbles rise is higher which lowers residence time and gas hold-up. With smaller bubbles, the gas hold-up and contact area between phases is larger and the mass transfer is enhanced and also the velocity of gas phase is lower.

The bubble size sensitivity analysis was added to error margin in each data point to give average error of 5%, which was calculated as average of error in iterations and error due to bubble size. The effect of bubble size on gas hold-up is shown in Figure 27a and on k_La in Figure 27b. Based on 3-point bubble sensitivity analysis in Figure 27a and 27b, hold-up and mass transfer rate follow 2nd degree polynomial curve in case average bubble size is used for simulations.
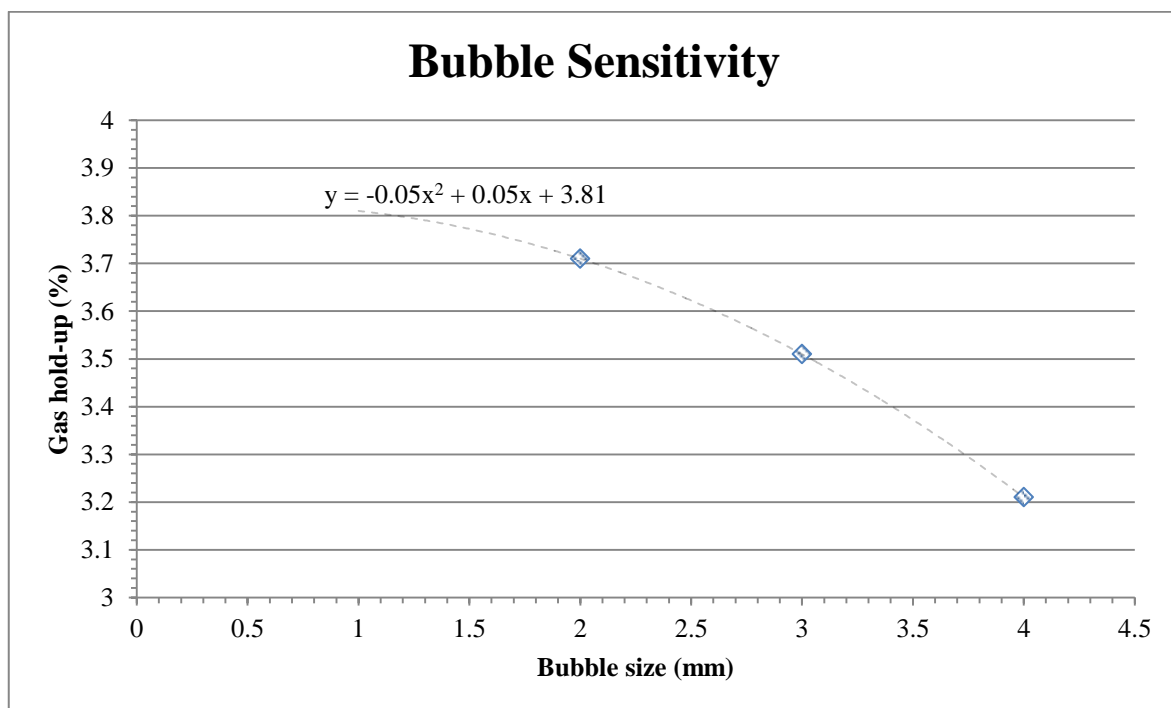
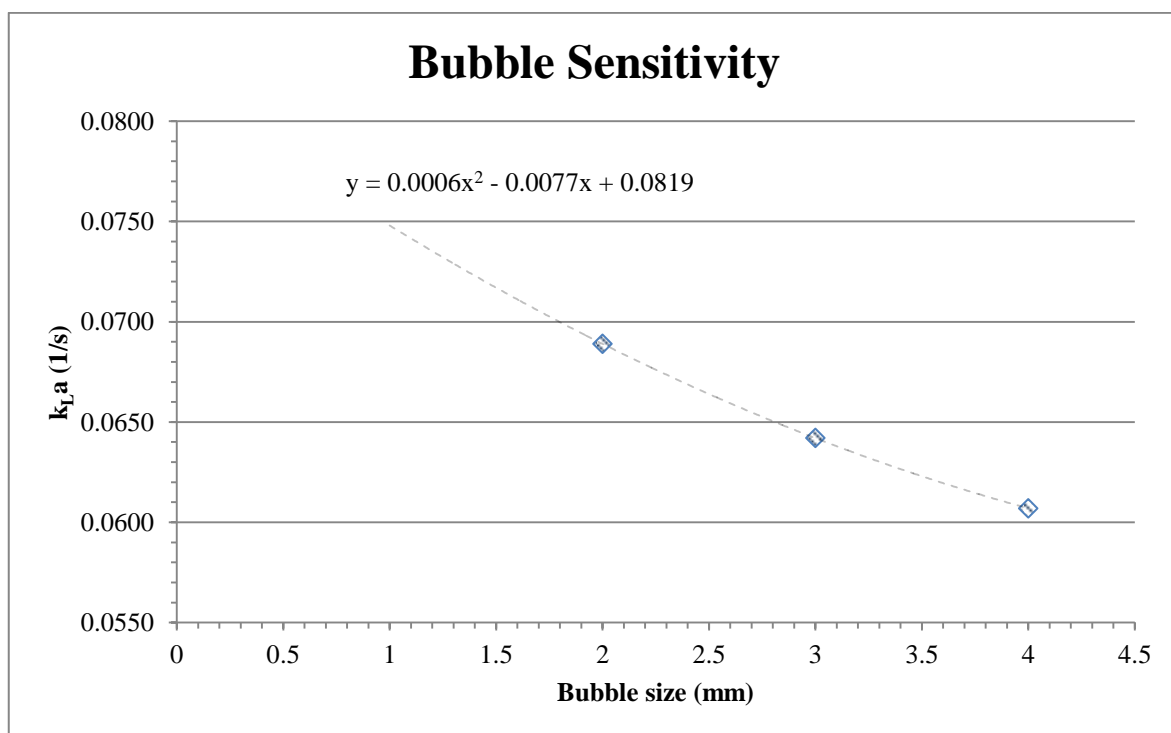**Figure 27a.** OKTOP®9000 reactor with 4020m^3/h gas feed with constant mixing intensity of 283W/m^3.

Figure 27b. OKTOP®9000 reactor with 4020m^3/h gas feed with constant mixing intensity of 283W/m^3.

8.3 Flooding

The flooding point was approximated by the correlation of Nienow *et al.* (1985) Eq. 31 in order to see how high gas feeds were needed for the flooding to occur. Based on Nienow's correlation a gas feed of 11700m^3/h should be enough to flood the impeller. However, one extra simulation was placed after 12000m^3/h just in case the flooding would occur at higher feed. The results are presented in Table XV.

Table XV. Simulation results for simulations done with Schiller-Naumann (Lane+Swarm). The flooding point is highlighted in orange.

d_B mm	Mixing speed 1/min	Q m^3/h	Gas feed vvm	Gas hold-up %	Torque Nm	P_G/V W/m^3	$k_L a$ 1/s	P_G/P_0 -
3	33	1980	0.0353	2.64	70400	260	0.0394	0.916
3	33	4020	0.0716	3.51	65800	243	0.0642	0.856
3	33	6000	0.1068	4.41	66600	246	0.0901	0.866
3	33	9000	0.1603	4.49	69200	255	0.1074	0.900
3	33	12000	0.2137	5.14	64900	240	0.1256	0.844
3	33	15000	0.2671	6.93	58300	215	0.1780	0.758

According on Nienow *et al.* (1985) impeller starts to flood when the ratio between gassed-to-ungassed (P_G/P_0) takes a step jump. In Table XV this occurs at 9000m^3/h, which would suggest that the flooding takes place somewhere near that point. This can also be seen in Figure 28. At 9000m^3/h the ratio is higher than those of 4020 and 6000m^3/h and after it begins to drop radically. This explains that the actual impeller can no longer control the gas flow properly.
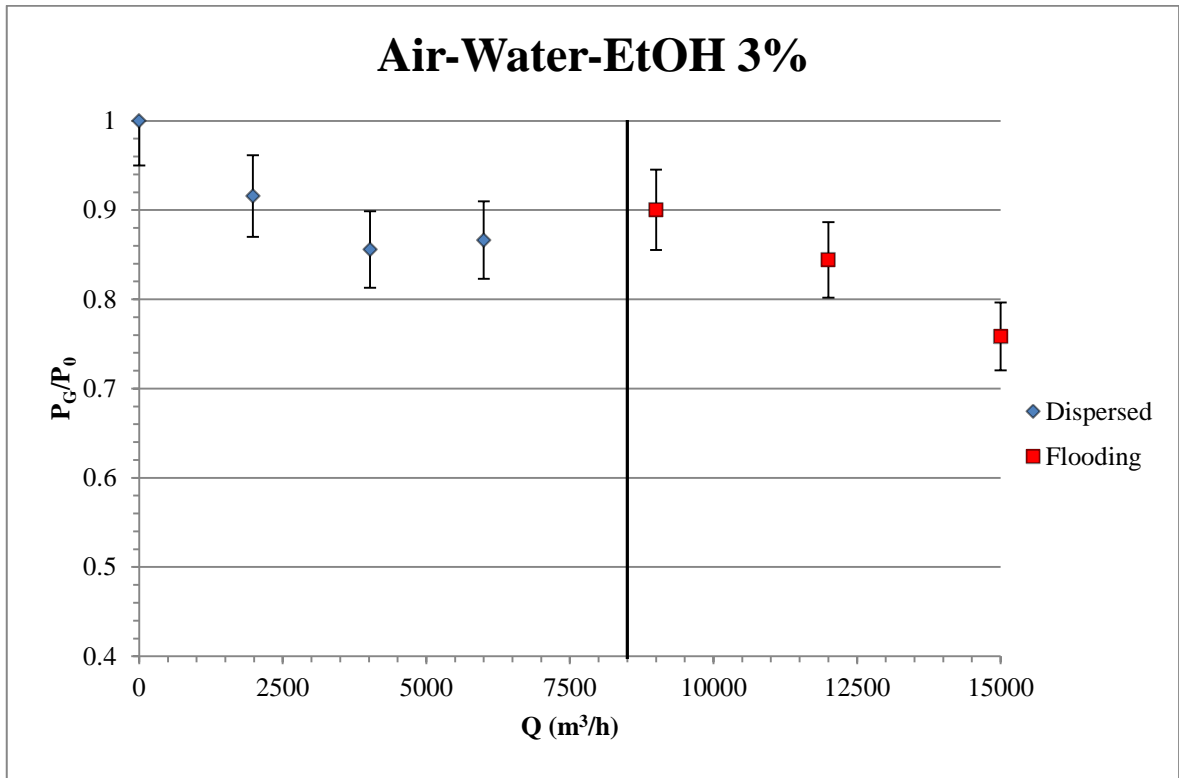
Figure 28. OKTOP®9000 reactor with various gas feeds with constant mixing intensity of 283W/m^3. The estimated flooding point is marked with a vertical line.

The calculated flooding threshold according to Nienow was around 11700m^3/h, which is higher than the flooding point witnessed in the Figure 28. However, based on study made by Takahashi and Nienow (1992) on the effect of gas density on power consumption in agitated aerated vessel using Nienow's correlation, they noticed that the correlation overestimates the flooding point. The line that is before flooding is estimated flooding point that is added to the rest of the charts in order to see the effect of flooding on the variables.

8.4 Gas Hold-up

When observing the average gas hold-up for the reactor as shown in Figure 29, it was noticed that there was hardly any change in the gas hold-up values between 6000 and 9000m^3/h gas feeds, which means that the impeller cannot properly disperse the gas anymore. At flow rates below 6000m^3/h the gas hold-up raises smoothly from 0 to ~4.4% and after 9000m^3/h it starts to rise again. This could be an indication that since the IBC model is used, the gas cannot go through impeller volume and normal flooding behavior

cannot be captured, where the gas would by-pass impeller and enter draft tube creating an opposite flow pattern in the reactor.
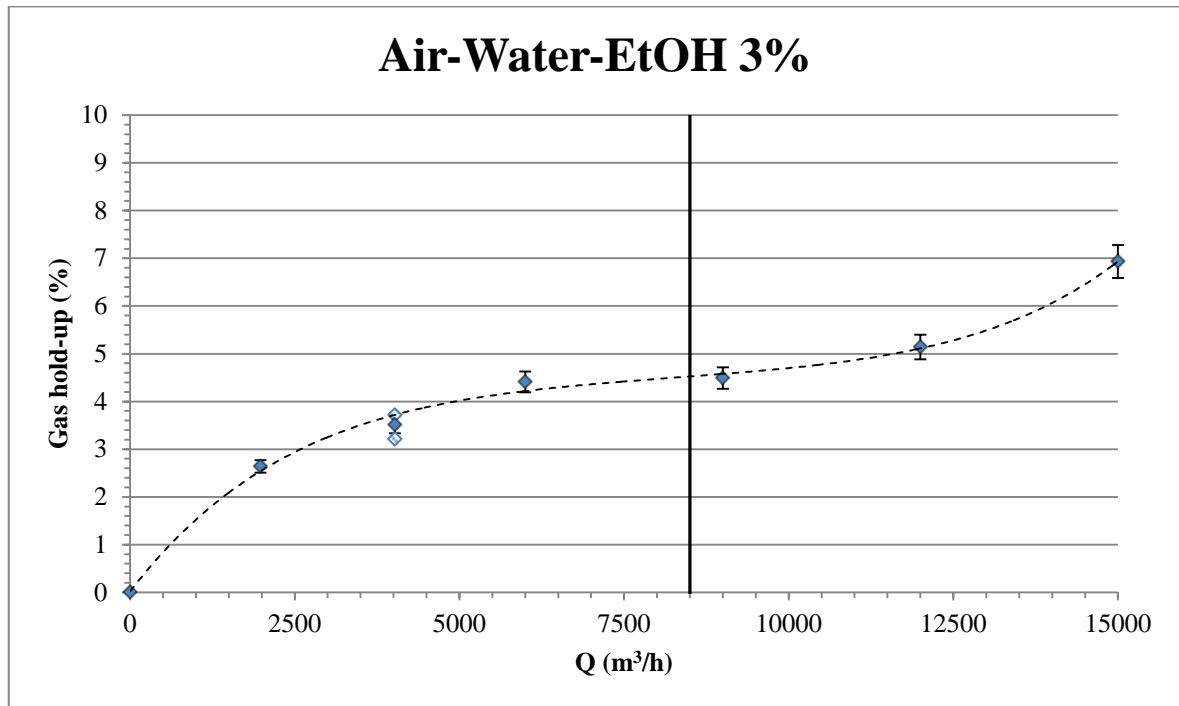

Figure 29. Behavior of gas inside the draft tube reactor with different gas feeds with constant constant mixing intensity of 283W/m^3. The estimated flooding point is marked with a vertical line.

8.5 Mass Transfer

The main focus of this study, mass transfer was studied in terms of using various gas feeds with constant impeller rotational speed. It is the most important variable in bioreactors in terms of production and also some cultivated microbes require certain level of mass transfer to take place in order to keep the population in the system alive. The mass transfer coefficient was calculated with Higbie's penetration model Eq.25, which is a function of turbulence dissipation energy and the interfacial area of bubbles Eq.26, which is a function of gas hold-up as bubble diameter is kept average. The results for mass transfer are presented in Figure 30. According to Figure 30, mass transfer seems to follow physical behavior as it starts to stabilize before the flooding point is reached. After the flooding point, the interfacial area takes over as the main driving force for mass transfer.
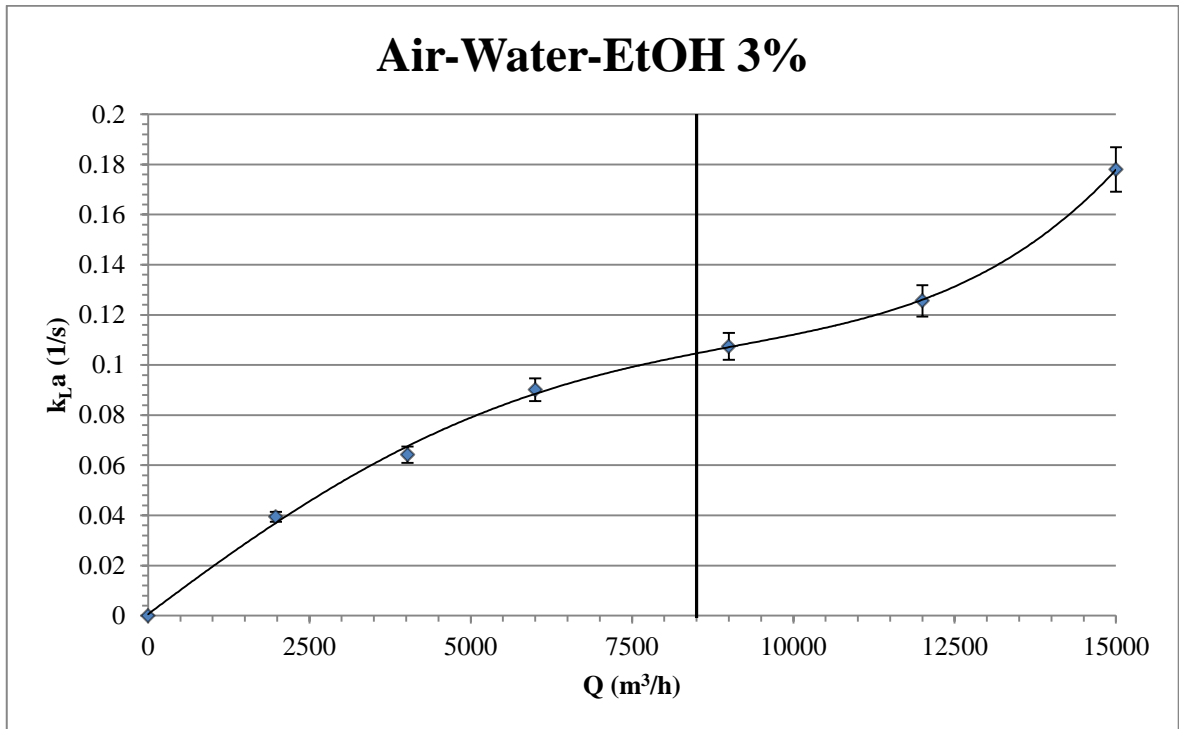
Figure 30. OKTOP®9000 reactor with various gas feeds with constant mixing intensity of 283W/m^3. The estimated flooding point is marked with a vertical line.

Based on the scale-up rules by Amanullah *et al.* (2004), geometrically similar vessels should provide similar results for mass transfer in case volumetric mixing intensity and superficial gas velocity are kept the same. Obviously this comes with a limitation of laboratory vessel flooding before higher superficial gas velocities can be achieved. In Figure 31 laboratory scale experiments made by Tervasmäki *et al.* (2016) are compared with the simulation results based on the scale-up rule.

There are slight differences in geometry as the ratio between the diameter and the height of the reactor are different for the industrial scale ($T/H_T = 0.34$) and laboratory scale (0.40), which may affect the results. Also the impeller spinarea (IBC model) grows with scale-up, which needs to be taken into account when comparing the results. Overall, the results between the two scales share similarities.

Tervasmäki *et al.* (2016) also made a correlation for mass transfer based on gas hold-up value for similar draft tube reactor in small scale. This was also taken into account when validating the results as can be seen in Figure 32. The simulated results agree with smaller gas hold-up values up to 3.51%, but start to diverge from the smaller scale values after that

point. Tervasmäki *et al.* stated that as the scale becomes larger such behavior is to be expected.
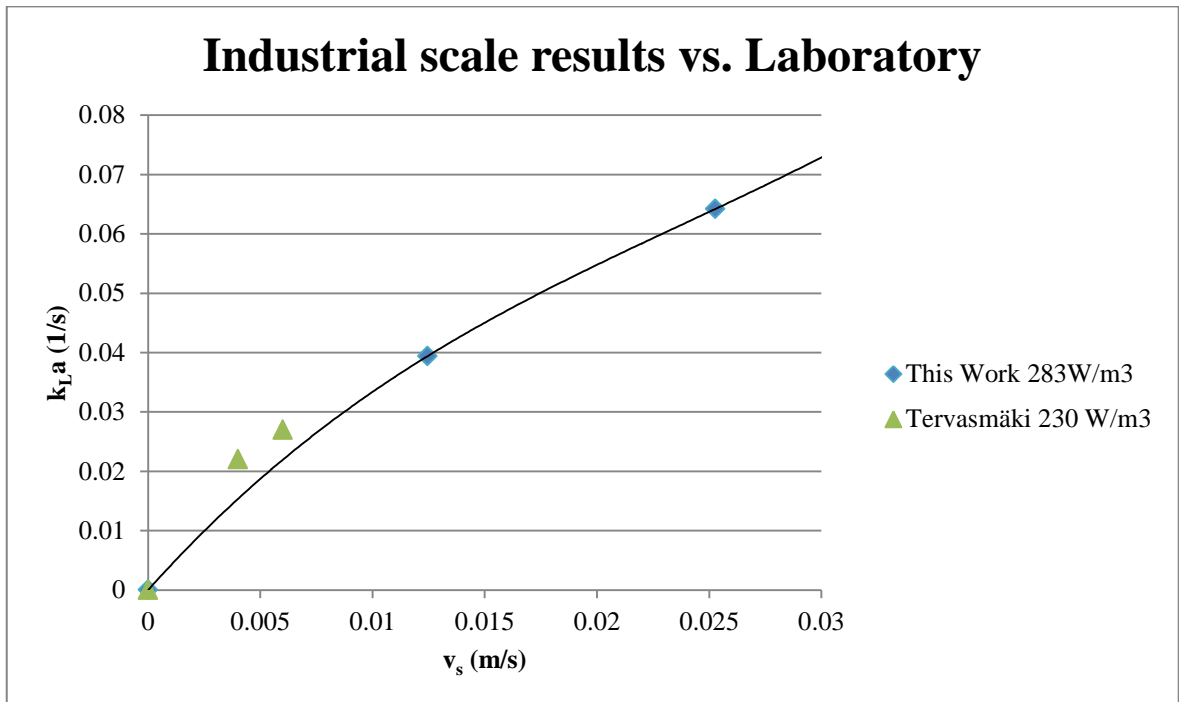

Figure 31. Comparison of laboratory scale reactor with similar volumetric mixing intensity and superficial gas velocity. (Tervasmäki *et al.* 2016)
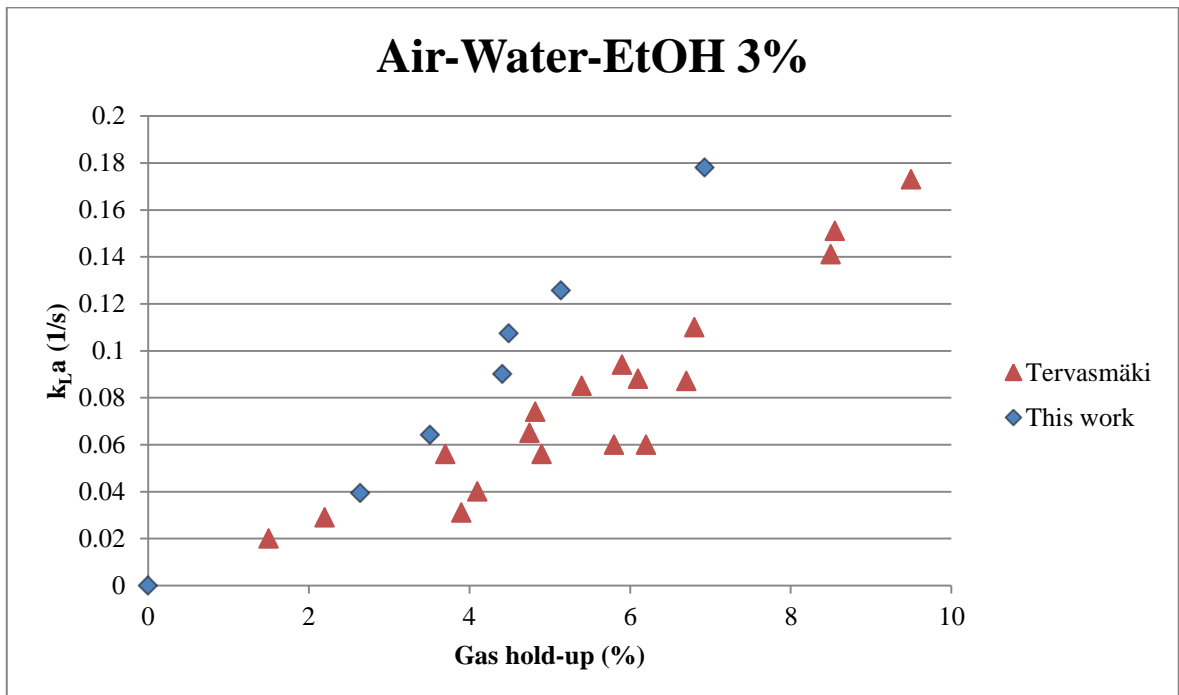

Figure 32. Comparison of mass transfer with the correlation based on gas hold-up made by Tervasmäki *et al.* (2016).

8.6 Visualization of the Results

ANSYS Fluent also offers visualization of the simulation results, which can support calculated results and also show how the gas is distributed inside the reactor as the gas feed is increased. Figure 33 shows the orientation of the vertical planes in Figure 34. On top of that, the local maximum gas hold-up values are presented in Table XVI to differentiate gas feed rates. $\alpha_{n,imp}$ represents the maximum local gas hold-up values near the impeller and $\alpha_{b,imp}$ values below impeller.
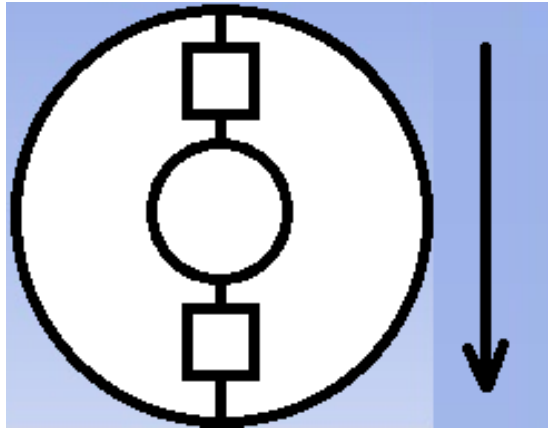

Figure 33.   Orientation of visualization from the top of the reactor. Squares are the lid holders and the circle in the middle is the top of the draft tube.

Table XVI.   Properties of draft tube reactor under constant impeller rotational speed. The local maximum values were probed from Fluent contour data.

Simulation case	Local maximum gas hold-up values				
	#5	#2	#6	#7	#8
Q (m³/h)	1980	4020	6000	9000	12000
$\alpha_{n,imp}$ (%)	15	20	25	35	42
$\alpha_{b,imp}$ (%)	10	15	20	25	28

It can be noticed from Table XVI that the local maximum gas hold-ups show linear growth of 5% per 2000m³/h, however after 6000m³/h the growth starts to decline as the impeller can no longer properly disperse the gas around it. The starting point of flooding is between 6000 and 9000m³/h.
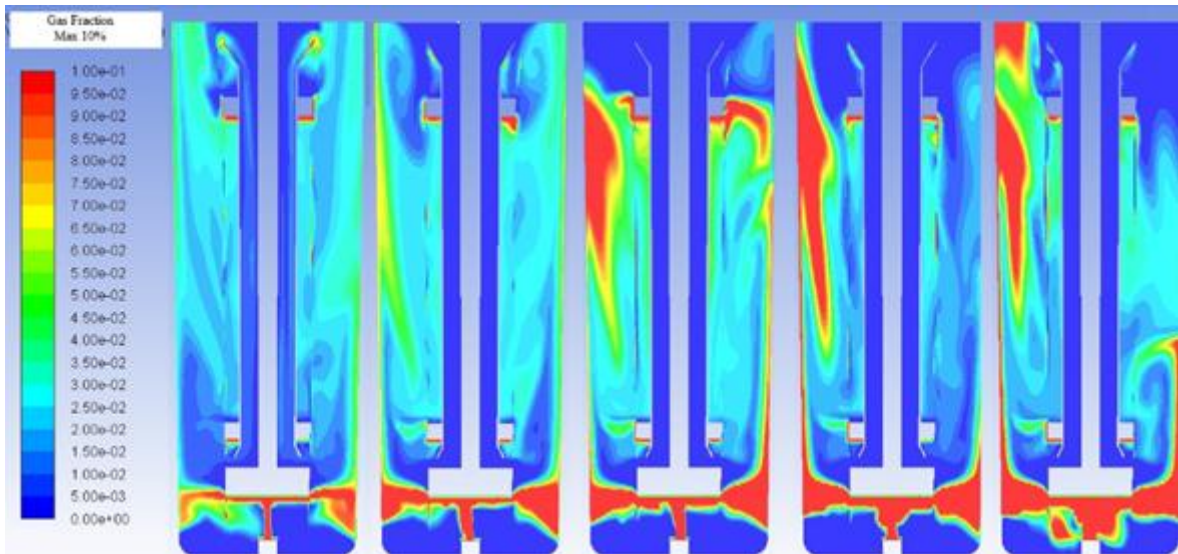
Figure 34.   Gas distribution inside the reactor with different gas feeds. Maximum gas fraction set as 10% to improve visualization. (Cases #5, #2, #6, #7 & #8 respectively)
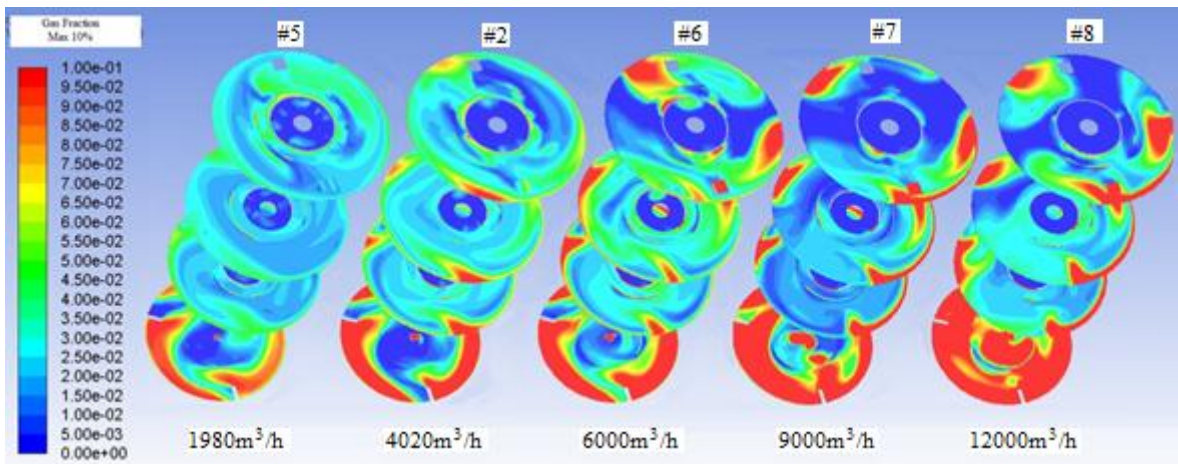
Figure 35.   Gas distribution inside the reactor with different gas feeds at different heights. Maximum gas fraction set as 10% to improve visualization. (Cases #5, #2, #6, #7 & #8 respectively)

Figure 35 shows how the gas is distribution between different horizontal planes, which are located at different heights from bottom of the reactor (below impeller) where the mixing is more intense to the top of the reactor (top of the draft tube).

Figure 34 and 35 support the simulated value for flooding point. After 4020m³/h (#2 base case) it can be seen that the gas no longer is distributed that well on top of the reactor. When the bottom of the reactor in Figure 35 is examined, the gas distribution loses its shape and with 12000m³/h the bottom is filled with gas. Same can be noticed from the higher planes, where the highest gas fractions are nearby the walls and do not distribute

uniformly in the annulus area. This is due to the gas axial velocity increasing with the effect of swarm due to higher gas fraction.

8.7 Additional Analysis

The flooding point of the impeller has been studied in this work and there was an approximation of 9000m^3/h gas flow simulated to represent the flooding point. The used IBC model might overestimate the flooding point and flooding might occur already with lower feed. Also the flooding of the draft tube would not occur even with higher feeds. This could be due to the fact that the IBC model does not see the growth of gas cavities behind impeller blades and blocks the route for gas to by-pass into the draft tube, which is not the case with MRF model. The benefit of IBC model however is more stable simulation compared to MRF model due to less complex geometric model.

The mass transfer values might also be lower due to underestimation of turbulence dissipation rates. Based on a study made by Deglon and Meyer (2006), turbulence dissipation rate gets underestimated in case of too coarse spatial discretization is used for simulations. The statement was supported by studies made by Wechsler *et al.* (1999) and Aubin *et al.* (2004).

9   CONCLUSIONS

In this study an industrial sized bioreactor was simulated. The steady-state gas-liquid simulations were based on a commercial reactor, OKTOP®9000, agitated draft tube reactor (985m^3). The geometry of the reactor was created in laboratory scale, which was then scaled-up with some modifications to improve simulation results. These modifications include raising the cell count, refining the first grid size near walls and limiting spinning area to keep the width to height ratio geometry of the impeller due to scale-up similar to the laboratory scale. The phases that were considered in the simulations were water-ethanol 3% solution (continuous phase, liquid) and air (dispersed phase, gas). The surface tension used for the simulations was based on experimental data from laboratory scale (Bogatenko 2017). The following objectives were the focus of this study:

- Performing study on drag laws that could be applied to the simulation process:

  There were not many drag models designed for large scale gas-liquid agitation reactors so assumptions had to be made on what were the driving forces in fluid movement. **(1)** In alcoholic solution bubbles get dispersed smaller than in pure water and rigid particles (bubbles) are less likely to coalesce compared to wobbling bubbles, which is why Schiller-Naumann was used for the simulations. **(2)** As an addition Lane's correlation that is based on experimental laboratory scale gas-liquid agitation vessel data was applied to Schiller-Naumann. **(3)** Since the size of the reactor increases, the amount of gas increases and the effect between the bubbles has a greater impact on the gas velocity, therefore the effect of swarm was implemented into Lane's correlation. This effect was studied by Roghair *et al.* (2013) in conditions that were suitable for this system.

- Making sensitivity analysis on the effect of bubble size:

  To reduce complexity of simulations, average bubble size of 3mm was chosen for the simulations based on study made by Laakkonen *et al.* (2007). The base case was simulated with 3±1mm range to see the impact on the major variables. The gas hold-up and $k_L a$ were in average range of ~7% from the results got with 3mm. It was noticed that the main variables of interest followed 2nd degree polynomial curve as the average bubble size was changed.

- Performing an analysis on the flooding point:

  Flooding point was calculated by Nienow *et al.* (1985) correlation ($11700\text{m}^3/\text{h}$), which was then identified to be ~23% lower ($9000\text{m}^3/\text{h}$). The flooding point could be seen from gassed-to-ungassed power having a step jump when compared with aeration number. This however was acceptable as a study made Takahashi and Nienow (1992) had also made same kind of observation, where the flooding point got overestimated with the correlation. It was also supported by the visualization of gas fraction distribution and the behavior of local maximum gas fraction values in terms of gas feed inside the reactor.

- Performing an analysis on how gas feed affects the mass transfer:

  The most important factor in a fermentation bioreactor is the mass transfer between the phases. This was studied by introducing gas feeds of 1980 to $15000 m^3/h$ into OKTOP®9000 draft tube reactor while keeping the impeller rotational speed constant. When average bubble size was used to calculate the mass transfer, the mass transfer rates seemed reasonable to the point of flooding (0.0394 to $0.1074s^{-1}$). Mass transfer rates are typically in the range 0.02 to $0.25s^{-1}$ for production scale fermenters (Doran 1995).

- Choosing the method for simulation that can be achieved in realistic computational time ($t_{computation} \leq 1$ week) :

  The chosen methods and mesh were appropriate for the set computational time limit as it took ~18 hours in total for one simulation.

Based on the results gained, there are some improvements that could be interesting to be applied for future studies. These include **(1)** the addition of gas solubility due to hydrostatic pressure, **(2)** more studies on gas-liquid behavior in industrial scale agitators to get better models to represent the fluid flow and **(3)** bubble size distribution model.

10 POSSIBILITIES FOR FUTURE APPLICATIONS

Based on literature review on other reactors and possibilities of 3D-printing, it might prove interesting to make smaller scale single-use-technology bioreactors based on the OKTOP®9000 model. This would require molding the structure of an OKTOP®9000 into a plastic bioprocess container (BPC). SUT bioreactors give flexibility to manufacturing and lower capital investments compared to stainless steel devices (Lopes 2015; Julien *et al.* 2016). Also, testing new processes with SUT bioreactors is easier than with conventional reactors. Regular SUT bioreactors deploy a sterilized bioprocess container into a stainless steel container. The BPC utilizes 3 Rushton turbines and the mixing is done by inserting an additional shaft into the motor. (ThermoFisher 2017) Since draft tube reactor has a better mass transfer in comparison to 3 Rushton turbine stirred tank reactor, it would lower the batch processing time. In case the fluid circulation is not to the standards and needs to be improved, a "net draft tube" might prove to be the solution to ensure even more superior mixing performance. A net draft tube is a wire-mesh draft tube, which makes liquid circulation better and increases the gas-liquid interfacial area. (Fu *et al.* 2003)

Another bioprocess, which OKTOP®9000 could be utilized in, would be arachidonic acid (ARA)-rich oil production by *Morierella alpina*. ARA belongs to omega-6 group of essential polyunsaturated fatty acids, which has broad applications in food industry, cosmetics, medicine and other fields. The process itself has a high oxygen demand and it is shear-sensitive, which are both pros of OKTOP®9000 reactor. (Nie *et al.* 2014)

Third idea would be to utilize OKTOP®9000 in wastewater treatment for poorly biodegradable wastewater, such as dyeing, pharmaceutical and tannery wastewater. Usually the wastewater treatment is poor due to low biogas production during the start-up period, which is caused by poor liquid circulation. Mixing, however, would provide a solution to this problem. (Wang *et al.* 2014)

One out of the box idea would be to use the reactor for pearl farming on the coastline or riverside since oysters require good water quality with adjustable salinity, 22-36m depth, fixed bed (net draft tube), slight water current that could be introduced from the river or sea current and algae for food (river also). (Haws 2002)

REFERENCES

Alzate-Hernandez, J.D. 2016. CFD simulation of an industrial FCC regenerator. Department of Processes and Energy, Bioprocesses and Reactive Flows, National University of Colombia, Medellín.

Amanullah, A. and Buckland, B.B. 2004. Mixing in the Fermentation and Cell Culture Industries. Chemical Engineering Handbook of Industrial Mixing Science Practice, Edited by Edward L. Paul, Victor A. Atiemo-Obeng and Suzanne M. Kresta: John Wiley & Sons, Inc.

Andersson, B., Andersson, R., Håkansson, L., Mortensen, M. Sudiyo, R. and van Wachem, B. 2012. Computational Fluid Dynamics for Engineers. University Press, Cambridge, United Kingdom.

ANSYS, Inc. 2016. ANSYS Fluent User's Guide. Release 18.0. SAS IP, Inc.

Atiemo-Obeng, V.A., Penney, W.R. and Armenante P. 2004. Solid-Liquid Mixing. Chemical Engineering Handbook of Industrial Mixing Science Practice, Edited by Edward L. Paul, Victor A. Atiemo-Obeng and Suzanne M. Kresta: John Wiley & Sons, Inc.

Aubin, J., Fletcher, D.F. and Xuereb, C. 2004. Modelling turbulent flow in stirred tanks with CFD: the influence of the modeling approach, turbulence model and numerical scheme. Experimental Thermal and Fluid Science 28, 431-445.

Bakker, A., Oshinowo, L. and Marshall, E.M. 2000. The Use of Large Eddy Simulation to Study Stirred Vessel Hydrodynamics. Proc. 10th European Conference on Mixing, Delft, The Netherlands, pp. 247-254.

Besagni, G., Inzoli, F. and De Guido, G. 2016. Experimental investigation on the influence of ethanol on bubble column hydrodynamics. Chem. Eng. Res. Des. 112, 1-15.

Blazek, J. 2005. Computational Fluid Dynamic: Principle and Applications, Chapter 3, Elsevier Science Publication, Oxford, UK.

Bogatenko, D. 2017. Analysis of volumetric mass transfer and overall gas hold-up in gas-liquid reactors relating to gas fermentation. Degree Program of Chemical Engineering, LUT School of Engineering Science, Lappeenranta University of Technology.

Brucato, A., Grisafi, F. and Montante, G. 1998. Particle drag coefficients in turbulent fluids. Chem. Eng. Sci. 57, 3185-3215.

Burns, A.D., Frank, T., Hamill, I. and Shi, J.-M. 2004. The Favre Averaged Drag Model for Turbulent Dispersion in Eulerian Multi-Phase Flows. 5th Int. Conf. on Multiphase Flow, ICMF'04. Paper No. 392. Yokohama, Japan.

Calderbank, P.H. 1959. Physical rate processes in industrial fermentations, Part-II. Trans. Inst. Chem. Eng. 37, 173-185.

Chisti, M.Y. and Moo-Young, M. 1988. Trans. Am. Inst. Chem. Eng, Prediction of liquid circulation velocity in airlift reactors with biological media. J. Chem. Technol. Biotechnol. 42, 211-219.

Deen, N.G., Sohlberg, T. and Hjertager, B.H. 2002. Flow generated by an aerated Rushton impeller: Two-phase PIV experiments and numerical simulations. Can. J. Chem. Eng. 80, 638-652.

Deglon, D.A. and Meyer, C.J. 2006. CFD modeling of stirred tanks: Numerical considerations. Minerals Engineering 19, 1059-1068.

Doran, P.M. 1995. Bioprocess Engineering Principles. London: Elsevier.

Elewuwa, F.A. 2016. Computational Modelling of Dimethyl Ether Separation and Steam Reforming in Fluidized Bed Reactors. PhD, Aston University.

Fu, C-C., Lu, S-Y., Hsu, Y-J., Chen, G-C., Lin, Y-R. and Wu, W-T. 2004. Superior mixing performance for airlift reactor with a net draft tube. Chem. Eng. Sci. 59, 3021-3028.

Gentric, C., Mignon, D., Bousquet, J. and Tanguy, P.A. 2004. Comparison of mixing in two industrial gas-liquid reactors using CFD simulations. Chem. Eng. Sci. 60, 2253-2272.

Haws, M. 2002. The basics of pearl farming: A layman's manual. Center for Tropical and Subtropical Aquaculture, Publication No. 127.

Hempel, D.C. and Dziallas, H. 1999. Scale-up, stirred tank reactors, in Encyclopaedia of Bioprocess Technology: Fermentation, Biocatalysis and Bioseparation, Vol. 3, M. C. Flickringer and S.W. Drew, eds., Wiley, New York, pp. 2314-2332.

Higbie, R. 1935. The Rate of Absorption of a Pure Gas into a Still Liquid During Short Periods of Exposure. vol. 31, pp. 365-389.

Holland, F. and Bragg, R. 1995. Fluid Flow for Chemical and Process Engineers 2nd edition. Butterworth-Heinemann.

Julien, C., Paldus, B.A., Langer, E., Blomberg, M., Ultee, M., Pora, H. and Balekai, S. 2016. Single-Use/Disposables Technologies and Equipment Roundtable. American Pharmaceutical Review.

Karimi, M., Akdogan, G., Dellimore, K.H. and Bradshaw, S.M. 2012. Comparison of Different Drag Coefficient Correlations in the CFD Modelling of a Laboratory-scale Rushton-turbine Flotation Tank. Ninth International Conference on CFD in the Minerals and Process Industries, CSIRO, Melbourne, Australia.

Khare, A., Singh, A. and Nokam, K. 2009. Best Practises in Grid Generation for CFD Applications Using HyperMesh. Hyperworks 2009 Presentations, India.

Khopkar, A.R. and Ranade, V.V. 2006. CFD Simulation of Gas-liquid Stirred Vessel: VC, S33 and L33 flow regimes. AlChE Journal 52, 1654-1672.

Koch, D.L and Subramanian, G. 2011. Collective Hydrodynamics of Swimming Microorganisms: Living Fluids. Annu. Rev. Fluid Mech. 43, 637-59.

Kulkarni, A. 2007. Mass transfer in bubble column reactors: effect of bubble size distribution. Ind. Eng. Chem. Res. vol. 46, no.7, pp. 2205-2211.

Laakkonen, M., Moilanen, P., Alopaeus, V. and Aittamaa, J. 2007. Modelling local bubble size distributions in agitated vessels. Chem. Eng. Sci. 62, 721-740.

Lane, G.L. 2006. Computational Modelling of Gas-liquid Flow in Stirred Tanks. PhD, University of Newcastle.

Launder, B.E. and Spalding, D.B. 1974. The numerical computation of turbulent flows. Comput. Meth. Appl. Mech. Eng. 3, 269-89.

Li, P., Lan, C., Xu, G., Lu, C. and Gao, J. 2009. Drag models for simulating gas-solid flow in the turbulent fluidization of FCC particles. Particuology vol. 7, no.4, 269-277.

Lopes, A.G. 2015. Single-use in the biopharmaceutical industry: A review of current technology impact, challenges and limitations. Food Bioprod. Process., vol. 93, pp. 98–114.

Luo, J.Y., Issa, R.I. and Gosman, A.D. 1994. Prediction of Impeller Induced Flows in Mixing Vessels Using Multiple Frames of Reference. Inst. Chem. Eng. Symp. Ser. 136, 549-556.

Luo, H.P. and Al-Dahhan, M.H. 2007. Macro-mixing in a draft-tube airlift bioreactor. Chem. Eng. Sci. 63, 1572-1585.

Machon, V., Pacek, A.W. and Nienow, A.W. 1997. Bubble sizes in electrolyte and alcohol solutions in a turbulent stirred vessel. Chem. Eng. Res. Des. 75, 339-348.

Maltby, R., Lewis, W., Wright, S., Smith, A. and Chew, J. 2016. Multiphase CFD Modelling of Single-Use-Technology Bioreactors for Industrial Biotechnology Applications. Proceedings of the 3rd International Conference on Fluid Flow, Heat and Mass Transfer (FFHMT'16), Paper No. 122, Ottawa, Canada.

Marshall, E.M. and Bakker A. 2004. Computational Fluid Mixing. Chemical Engineering Handbook of Industrial Mixing Science Practice, Edited by Edward L. Paul, Victor A. Atiemo-Obeng and Suzanne M. Kresta: John Wiley & Sons, Inc.

McNaught, A. D. and Wilkinson, A. 1997. IUPAC. Compendium of Chemical Terminology, 2nd ed. (the "Gold Book"). Compiled by Blackwell Scientific Publications, Oxford. XML on-line corrected version: http://goldbook.iupac.org (2006-) created by Nic, M., Jirat, J. & Kosata, B.; updates compiled by A. Jenkins.

Metzner, A.B. and Taylor, J.S. 1960. Flow patterns in agitated vessels. AlChE J. 6, 109-114.

Middleton, J.C. 1992. Gas-liquid dispersion and mixing, Mixing in the Process Industries, eds. Harnby, N., Edwards, M.F., Nienow, A.W., Butterworth-Heinemann, Oxford, pp. 322-363.

Middleton, J.C. and Smith, J.M. 2004. Gas-Liquid Mixing in Turbulent Systems. Chemical Engineering Handbook of Industrial Mixing Science Practice, Edited by Edward L. Paul, Victor A. Atiemo-Obeng and Suzanne M. Kresta: John Wiley & Sons, Inc.

Nagata, S. 1975. Mixing: Principles and Applications, Haltead Press, New York.

Nie, Z.K., Ji, X.J., Shang, J.S., Zhang, A.H., Ren, L.J and Huang, H. 2014. Arachidonic acid-rich oil production by *Mortiella alpina* with different gas distributors. Bioprocess Biosyst. Eng. 37, 1127-1132.

Nienow, A.W., Warmoeskerken, M.M.C.G., Smith, J.M. and Konno, M. 1985. The Flooding/Loading Transition and the Complete Dispersal Condition in Aerated Vessels Agitated by a Rushton Turbine. Proc. 5th Europ. Conf. on Mixing, Paper 15, pp. 143.

Oldshue, J. Y. 1966. Fermentation mixing scale-up techniques, Biotechnol. Bioeng., 8, 3-24.

Oosterhuis, N.M.G. 1984. Scale up of bioreactors: a scale down approach, Ph.D. dissertation, Delft University of Technology, The Netherlands.

Oosterhuis, N.M.G. and Kossen, N.W.F. 1984. Dissolved oxygen concentration profiles in a production scale bioreactor, Biotechnol. Bioeng., 26, 546-550.

Outotec Oyj, Available at: http://www.outotec.com/products/leaching-and-solution-purification/zinc-concentrate-direct-leaching/ [Accessed 30.10.2017]

Patel, G.N. 2010. CFD Simulation of Two-phase and Three-phase Flows in Internal-loop Airlift Reactors. Department of Mathematics and Physics, Faculty of Technology, Lappeenranta University of Technology.

Patterson, G.K., Paul, E.L., Kresta, S.M. and Etchells III, A.W. 2004 Mixing and Chemical Reactions. Chemical Engineering Handbook of Industrial Mixing Science Practice, Edited by Edward L. Paul, Victor A. Atiemo-Obeng and Suzanne M. Kresta: John Wiley & Sons, Inc.

Roghair, I., Van Sint Annaland, M. and Kuipers, H.J.A.M. 2013. Drag force and clustering in bubble swarms. AIChE J, 59: 1791–1800.

Roussinova, V.T., Grgic, B. and Kresta, S.M. 2000. Study of Macro-instabilities in Stirred Tanks Using a Velocity Decomposition Technique. Chem. Eng. Res. Des., 78, 1040-1052.

Scargiali, F., D'Orazio, A., Grisafi, F. and Brucato, A. 2007. Modelling and Simulation of Gas-liquid Hydrodynamics in Mechanically Stirred Tanks. Trans. IChemE, Part A, Chem. Eng. Research and Design, 85(A5), 637-646.

Schiller, L. and Naumann, A. 1935. A drag coefficient correlation. Zeitschrift des Vereins Deutscher Ingenieure, vol. 77, 318-320.

Shih, T.-H., Liou, W.W., Shabbir, A., Yang, Z. and Zhu, J. 1995. A New k-ε Eddy Viscosity Model for High Reynolds Number Turbulent Flows. Computers & Fluids 24(3), 227–238.

Skelland, A.H.P. and Ramsay, G.G. 1987. Minimum Agitation Speed for Complete Liquid-Liquid Dispersion. Ind. Eng. Chem. Res., vol. 26, pp. 77 − 81.

Smith, J.M. 1985. Dispersion of gases in liquids, Chapter 5 in Mixing of Liquids by Mechanical Agitation, J. J. Ulbrecht, and G. K. Patterson, eds., Gordon & Breach, New York.

Smith, J.M., Warmoeskerken, M.M.C.G. and Zeef, E. 1987. Flow Conditions in Vessels Dispersing Gases in Liquids with Multiple Impellers. Biotechnology Processes, C.S. Ho and J.Y. Oldshue, eds., AlChE, New York, pp. 107-115.

Takahashi, K. and Nienow, A.W. 1992. Effect of Gas Density on Power Consumption in Aerated Vessel Agitated by a Rushton Turbine. Jour. Chem. Eng. Japan 25, pp. 432-433.

Tervasmäki, P., Latva-Kokko, M., Taskila, S. and Tanskanen, J. 2016. Mass transfer, gas hold-up and cell cultivation studies in a bottom agitated draft tube reactor and multiple impeller Rushton turbine configuration. Chem. Eng. Sci., 155, 83-98.

ThermoFisher Scientific. Single-Use Bioprocessing Equipment. Available at: https://www.thermofisher.com/fi/en/home/life-science/bioproduction/single-use-bioprocessing/single-use-equipment.html [Accessed 09.11.2017]

Tiainen, J. 2014. Modeling of Liquid-Solid Flow in Industrial Scale. Degree Programme in Energy Technology, Faculty of Technology, Lappeenranta University of Technology.

Treybal, E. 1966. Liquid Extractor Performance. Chem. Eng. Prog., 62(9), pp. 67–75. Perry's Chemical Engineers' Handbook, 8th Edition, Perry, R.H., Green, D.W. 2008.

Tsao, G.T. 2014. Annual Reports on Fermentation Processes, vol. 6. Elservier, 160-169.

Van't Riet, K. 1979. Review of measuring methods and results in nonviscous gas-liquid mass transfer in stirred vessels, Ind. Eng. Chem. Process. Des. Dev., 18(3), 357-363.

Versteeg, H.K. and Malalasekera, W. 2007. An Introduction to Computational Fluid Dynamics: The Finite Volume Method. Pearson Education.

Wang, L.P. and Stock, D.E. 1993. Dispersion of Heavy Particles by Turbulent Motion. Department of Mechanical and Material Engineering, Washington State University, Pullman, Washington.

Wang, H. and Zhai, Z. 2012. Analyzing grid independency and numerical viscosity of computational fluid dynamics for indoor environment applications. Building and Environment 52, 107-118.

Wang, J., Xu, W., Yan, J. and Yu, J. 2014. Study on the flow characteristics and the wastewater treatment performance in modified internal circulation reactor. Chemosphere 117, 631-637.

Wechsler, H., Breuer, M. and Durst, F. 1999. Steady and unsteady computations of turbulent flows induced by a 4/45° pitched-blade impeller. ASME Journal of Fluids Engineering, 121, 318-328.

Zhang, Z. and Chen, Q. 2007. Comparison of the Eulerian and Lagrangian methods for predicting particle transport in enclosed spaces. Atmospheric Environment 41(25), 5236-5248.